in acute promyelocytic leukemia, and that the repressor complexes, including HDACs itself, as well as RAR, are the molecular target of retinoic acid in differentiation therapy (28–32).

Xeroderma pigmentosum group A (XPA)–binding protein 2 (XAB2), which we independently isolated under the name of HDART[7] by virtue of its sequence similarity to *Drosophila* CRN, is composed of 855 amino acids. XAB2 contains 15 tetratricopeptide repeat motifs and functions in a nucleotide excision repair complex (33). Cloned by virtue of its ability to interact with XPA protein in the yeast two-hybrid system, XAB2 thus derives its name as XPA-binding protein 2, and is found to form a complex with the nucleotide excision repair machinery (33). XAB2 knockout mice have been reported to show preimplantation lethality (34, 35). Xeroderma pigmentosum is a rare human hereditary disease characterized by hypersensitivity to sunlight, a high incidence of skin cancer in sun-exposed areas, and accelerated neurodegeneration (36, 37). Cells from xeroderma pigmentosum patients are hypersensitive to killing by UV irradiation, with early development of skin cancer being caused by defective DNA repair (38–41). Preneoplastic diseases including xeroderma pigmentosum were previously shown to be successfully treated with retinoids (1, 4). Expanding on these observations, we focus in this article on the role of XAB2 as a novel target for retinoic acid–based differentiation therapy for cancers, defining in particular the biological and physiologic function of XAB2 in the RAR/HDAC3 complex. We now show that XAB2 functions as a corepressor of the RAR/HDAC3 complex, and that knockdown of XAB2 by small interfering RNA (siRNA) enhances sensitivity to ATRA in the acute promyelocytic leukemia cell line HL60 and the rhabdomyosarcoma cell line MM-1-19P, as well as the ATRA-resistant neuroblastoma cell line IMR-32.

Materials and Methods

Cells, antibodies, and reagents. HEK293T, HepG2, HL60, and MM-1-19-P were grown in DMEM (Life Technologies, Inc., Grand Island, NY) supplemented with 10% heat-inactivated fetal bovine serum (FBS; Life Technologies), 100 units/mL penicillin, and 100 μg/mL streptomycin (Life Technologies). MM-1-19-P human rhabdomyosarcoma cell line, HL60 human promyelocytic leukemia cell line, and retinoic acid–resistant human neuroblastoma cell line IMR-32 were grown in RPMI 1640 (Life Technologies) supplemented with 10% FBS, 100 units/mL penicillin, and 100 μg/mL streptomycin, using Laminin six-well multiwell plates (BD Biosciences, San Jose, CA).

The following antibodies were purchased from Santa Cruz Biotechnology, Inc. (Santa Cruz, CA): anti-Flag M2 monoclonal antibody (mAb), anti–green fluorescent protein (GFP) polyclonal antibody (pAb), antitubulin mAb, anti-HDAC1 pAb, anti-HDAC3 pAb, anti-HDAC4 pAb, anti-HDAC6 pAb, anti-RARα pAb, Texas red–conjugated antigoat immunoglobulin secondary antibody, Texas red–conjugated antimouse immunoglobulin secondary antibody, and FITC-conjugated antimouse immunoglobulin secondary antibody. Anti-XAB2 mAb was purchased from Abnova (Taipei, Taiwan); anti-XAB2 polyclonal antibody was obtained from Mo Bi Tec (Goettingen, Germany); phycoerythrin-conjugated CD11b and 7-amino-actinomycin D were obtained from BD PharMingen (San Jose, CA); and anti–acetyl-histone H4 polyclonal antibody was obtained from Upstate (Chicago, IL).

siRNA against human XAB2. We selected the target sequences from +90 to +108 and +1,673 to +1,691 downstream of the start codon of human XAB2 mRNA (National Center for Biotechnology Information accession no. NM_020196; sense siRNA ss1, 5′-GAACCAAUUCUCUGUCAAAdTdT-3′; sense siRNA ss2, 5′-GUAUUTAUUTGAUUAAATTdTdT-3′). Moreover, control siRNA was prepared to examine nonspecific effects of siRNA duplexes (5′-GAACACUACUUCGUUCAAAdTdT-3′). These selected sequences also were submitted to a BLAST search against the human genome sequence to ensure that only one gene of the human genome was targeted. siRNAs were purchased from Japan Bioservice (Saitama, Japan). siRNA duplex formation (annealing) was done as previously described (42). A total of 60 pmol of siRNA duplexes were transfected into 0.5×10^6 cells using Nucleofector (Amaxa, Inc., Gaithersburg, MD). After 48 h of transfection, cells were prepared for examination.

Cellular differentiation. MM-1-19-P cells (1×10^6/mL) were transfected with 2 μg of pcDNA3-XAB2 or pcDNA3 plasmids as mock control, and pEGFP-C1 plasmid (0.4 μg) was cotransfected for the identification of transfected cells. After 24 h of transfection, cells were treated with 2 μmol/L ATRA for an additional 24 h and were submitted to fluorescence microscopy analysis. The effect of exogenous XAB2 on cells was observed by morphologic analysis of cells through the use of phase-contrast microscopy merged with green fluorescence of GFP. Myocytic differentiation of rhabdomyosarcoma cells was observed with phase-contrast microscopy, with two pathologists identifying the morphologic changes to myocytic differentiation. For quantification, the percentage of GFP-positive, myocyte-differentiated cells among a total of 1,000 GFP-positive cells was shown in the graph. All experiments were done in triplicate and the results presented as means with SE.

After transfection of siRNA, IMR-32 cells (1×10^6/mL) were incubated in the presence of 2 μmol/L ATRA for an additional 48 h. Neuroganglional differentiation of neuroblastoma cells was observed as previously described (43); cells with extending processes longer than twice the diameter of the cell body were counted as being differentiated, with two pathologists identifying the morphologic changes to formation of neurite-like outgrowth. For quantification, the percentage of differentiated cells among 1,000 cells was shown in the graph. All experiments were done in triplicate and the results presented as means with SE.

Relative quantitative reverse transcription-PCR assay. In experiments assessing expression of RARβ and CYP26 mRNA, after HEK293T or HL60 cells were treated as described above, total RNA was then extracted and cDNA was produced as previously described (44). PCR primers for the coding sequences of RARβ and CYP26 were as follows: RARβ, forward 5′-ATGTTTGACTGTATGGATGTT-3′, reverse 5′-CCCACTTCAAAGCACTTCTG-3′; CYP26, forward 5′-GATGAAGCGCAGGAAATAC-3′, reverse 5′-ATGGC-GATTCGGAACATGGAG-3′. These primers were designed for the coding sequences that are located on different exons to eliminate amplifying genomic DNA contamination in the PCRs. The quantities of mRNA were adjusted equally by using PCR of β-actin (forward primer 5′-CAAGA-GATGGCCACGGCTGCT-3′ and reverse primer 5′-TCCTTCTGCATCC-TGTCGGCA-3′ as the internal control).

Chromatin immunoprecipitation assay. Chromatin immunoprecipitation assay was done using 1×10^6 of HL60 cells in the presence or absence of 1 μmol/L ATRA for 72 h. Protein-DNA complexes were prepared using EZ ChIP Chromatin Immunoprecipitation Kit (Upstate) according to the manufacturer's instruction. After washing and reverse cross-linking, immunoprecipitated DNA was purified and PCR was done. The following PCR primers were used to detect the immunoprecipitated promoter DNA: RARβ promoter, forward 5′-CTCTGGCTGTCTGCTTTTGC-3′, reverse 3′-CAAAAAGCCTTCCGAATGC-3′; CYP26 promoter, forward 5′-TAAA-GATTTTGGGCAGCG-3′, reverse 5′-CATCTGCAAGGTTTCCCCAA-3′. The PCR reactions were done as described above.

Coimmunoprecipitation assay. For coimmunoprecipitation assays involving endogenous XAB2 and HDACs, nuclear extracts were prepared from 1×10^7 HL60 cells as previously described (45). Nuclear extracts were then isolated by centrifugation at 15,000 × *g* for 30 min. Immunoprecipitation assays were done subsequently by incubating nuclear extracts with 2 μg of control immunoglobulin and protein G-Sepharose beads (Amersham Pharmacia, Piscataway, NJ) at 4°C for 1 h. After centrifugation, supernatants were incubated with 2 μg of anti-XAB2 mAb at 4°C for 1 h, followed by the addition of protein G-Sepharose beads for 1 h (45). Cell lysates and nuclear extracts were prepared and coimmunoprecipitation assay, SDS-PAGE, and

[7] Unpublished observation.

Western blot analysis were conducted according to the methods described elsewhere (44, 45).

Confocal laser microscopy. For fluorescence microscopy experiments, HL60 cells were incubated for 24 h in the presence or absence of ATRA and then attached to microslide glass (Matsunami Glass, Inc., Tokyo, Japan) coated with poly-L-lysine and fixed with ice-cold acetone/methanol (1:1). After washing with ice-cold PBS, cells were blocked with mouse and goat immunoglobulin isotypes, followed by incubation with anti-XAB2 mAb, RARα pAb, or anti-HDAC3 pAb (each at a concentration of 10 μg/mL), then washed and incubated with FITC-conjugated antimouse immunoglobulin and/or Texas red–conjugated antigoat immunoglobulin antibodies (each at a concentration of 5 μg/mL). Confocal microscopy was done as described elsewhere (44, 45).

Chloramphenicol acetyltransferase assay. To examine the potential effect of XAB2 on ATRA-mediated transcriptional activity, HepG2 cells were transiently transfected with pRARE-chloramphenicol acetyltransfelase (CAT), which is a RARE-containing RAR reporter plasmid, cloned in frame with CAT under the control of a thymidine kinase minimal promoter. Cells were seeded onto 35-mm-diameter dishes at a density of 1.75×10^5 per well and incubated overnight in FCS-supplemented medium. The following day, cells were transfected with pRARE-CAT (1 μg), pSV-β-gal (0.5 μg), and pcDNA3-XAB2 (0.5 or 1.0 μg), or pcDNA3 as mock control. The amount of expression vector was adjusted to 1 μg with pcDNA3 empty vector in each transfection. Twenty-four hours later, culture medium was removed and cells were washed thrice with serum-free MEM (Life Technologies), and then treated with fresh medium containing 100 nmol/L ATRA. Cells were harvested after 24 h and assayed for β-galactosidase and CAT activity with the use of the β-Galactosidase Enzyme Assay System (Promega, Madison, WI) and CAT Enzyme Assay System (Promega) according to the manufacturer's instruction. For transfection efficiency, CAT activity was normalized to β-galactosidase activity. The CAT activity in control cells treated with DMSO vehicle and a mock vector was set as equal to one and all other values are expressed as fold induction. Data represent mean from triplicate experiments ± SE.

Statistics. Student's *t* test was used to determine whether the difference between control and experimental samples was significant ($P < 0.05$).

Results

Overexpression of XAB2 inhibits cellular differentiation and transcriptional activation induced by ATRA. To determine an effect of XAB2 on cellular differentiation, we first examined whether cellular differentiation is induced by overexpression of exogenous XAB2. For this purpose, we used the human rhabdomyosarcoma cell line MM-1-19-P, which is mainly composed of small polygonal cells and terminally differentiates to myotube-like giant cells following treatment with ATRA (46). As shown in Fig. 1*A*, MM-1-19-P cells transfected with mock vector differentiated to myotube-like giant cells following treatment with ATRA (*arrowheads* in *a*). On the other hand, ATRA did not induce any morphologic changes in MM-1-19-P cells transfected with XAB2 expression plasmid (Fig. 1*A*, *b*). For further confirmation and quantification of ATRA-induced cellular differentiation of MM-1-19-P cells, we next conducted cotransfection experiments with XAB2-expressing plasmids (pcDNA3-XAB2) or mock plasmid (pcDNA3) and GFP-expressing plasmids (pEGFP-C1) for visualization. As shown in Fig. 1*B*, no change was observed both in MM-1-19-P cells transfected with mock and GFP-expressing plasmids and in MM-1-19-P cells transfected with XAB2- and GFP-expressing plasmids (*a* and *c*). On the other hand, myocytic cellular differentiation following treatment with ATRA was significantly observed in mock-transfected MM-1-19-P cells, which were cotransfected with GFP-expressing plasmid (Fig. 1*B*, *b*). However, cellular differentiation to myotube-like giant cell induced by ATRA was not detected in MM-1-19-P cells transfected with XAB2 expression plasmid (Fig. 1*B*, *d*). To quantify the number of ATRA-induced differentiated cells in the mock- and XAB2-transfected MM-1-19-P cell population, we counted the myotube-like giant cells expressing GFP under examination by fluorescence and bright-field microscopy. As shown in Fig. 1*C*, MM-1-19-P cells transfected with mock and GFP vectors exhibited an increase in the number of differentiated cells (Fig. 1*C*, #). However, ATRA-induced differentiation of XAB2-transfected MM-1-19-P cells was significantly inhibited (Fig. 1*C*, ##). These results suggest that XAB2 has an inhibitory effect on ATRA-mediated cellular differentiation.

To confirm the inhibitory effect of XAB2 on ATRA-induced cell differentiation, CAT assays were done with the RAR reporter plasmid containing a RARE under the control of a thymidine kinase minimal promoter (pRARE-CAT). HepG2 cells were transiently transfected with pcDNA3-XAB2, which allows for the constitutive expression of XAB2, and were grown in the presence or absence of ATRA. In mock (pcDNA3)-transfected cells, CAT activity was induced 5-fold by ATRA. However, the ATRA-induced CAT activation was suppressed in a dose-dependent manner by XAB2 (Fig. 1*D*). These results suggest that XAB2 suppresses ATRA-activated transcription.

To further determine whether the overexpressed XAB2 protein plays an inhibitory role in ATRA-induced activation of transcription, we analyzed ATRA-targeted gene expression pattern in HEK293T cells by reverse transcription-PCR (RT-PCR). For this purpose, two RARα target genes, *RARβ* and *CYP26*, were selected (47). HEK293T cells were transiently transfected with pcDNA3-XAB2 to allow for the constitutive expression of XAB2 and were grown in the presence or absence of ATRA. Total RNA was purified and RT-PCR using RARβ-, CYP26-, and β-actin-specific primers was done. As shown in Fig. 1*E*, in mock (pcDNA3)-transfected cells, endogenous RARβ and CYP26 mRNA expression was induced by ATRA (*lanes 1* and *2*). However, the ATRA-induced RARβ and CYP26 expression was suppressed in a dose-dependent manner by XAB2 (Fig. 1*E*, *lanes 3–6*). Exogenous XAB2 transfection did not affect the expression level of endogenous RARβ and CYP26 mRNA (Fig. 1*E*, *lanes 1*, *3*, and *5*). These results confirm our earlier data indicating that XAB2 suppresses ATRA-activated gene transcription.

Knockdown of XAB2 by siRNA enhances cellular differentiation of HL60 cells induced by ATRA. To further define an inhibitory effect of XAB2 on ATRA-induced cellular differentiation, we next used the human promyelocytic leukemia cell line HL60, which is induced to differentiate to neutrophilic cells by various drugs including ATRA (48). For this purpose, we prepared two separate siRNA against XAB2, as described in Materials and Methods, to ensure the specificity of the knockdown effect. As shown in Fig. 2*A*, these siRNAs against XAB2 (ss1 and ss2) effectively knocked down XAB2 expression in HL60 cells (*top, lanes 2* and *4*). Because XAB2 in HL60 cells was not significantly knocked down by control siRNA (Fig. 2*A*, *top, lanes 1* and *3*) and expression level of tubulin as a housekeeping protein was not affected by both of siRNAs (Fig. 2*A*, *bottom*), this inhibitory effect of XAB2 by siRNAs in HL60 cells was specific. In addition, the expression levels of HDAC3 and RARα were not changed in the presence or absence of siRNA treatment (data not shown). We next examined ATRA-induced cellular differentiation of HL60 cells in the presence or absence of siRNAs against XAB2 through flow cytometric analysis of cell-surface expression level of CD11b (49). As shown in Fig. 2*B*, ATRA-induced HL60 cell differentiation was enhanced in a dose-dependent manner with treatment with siRNAs against XAB2 as compared with the level of differentiation

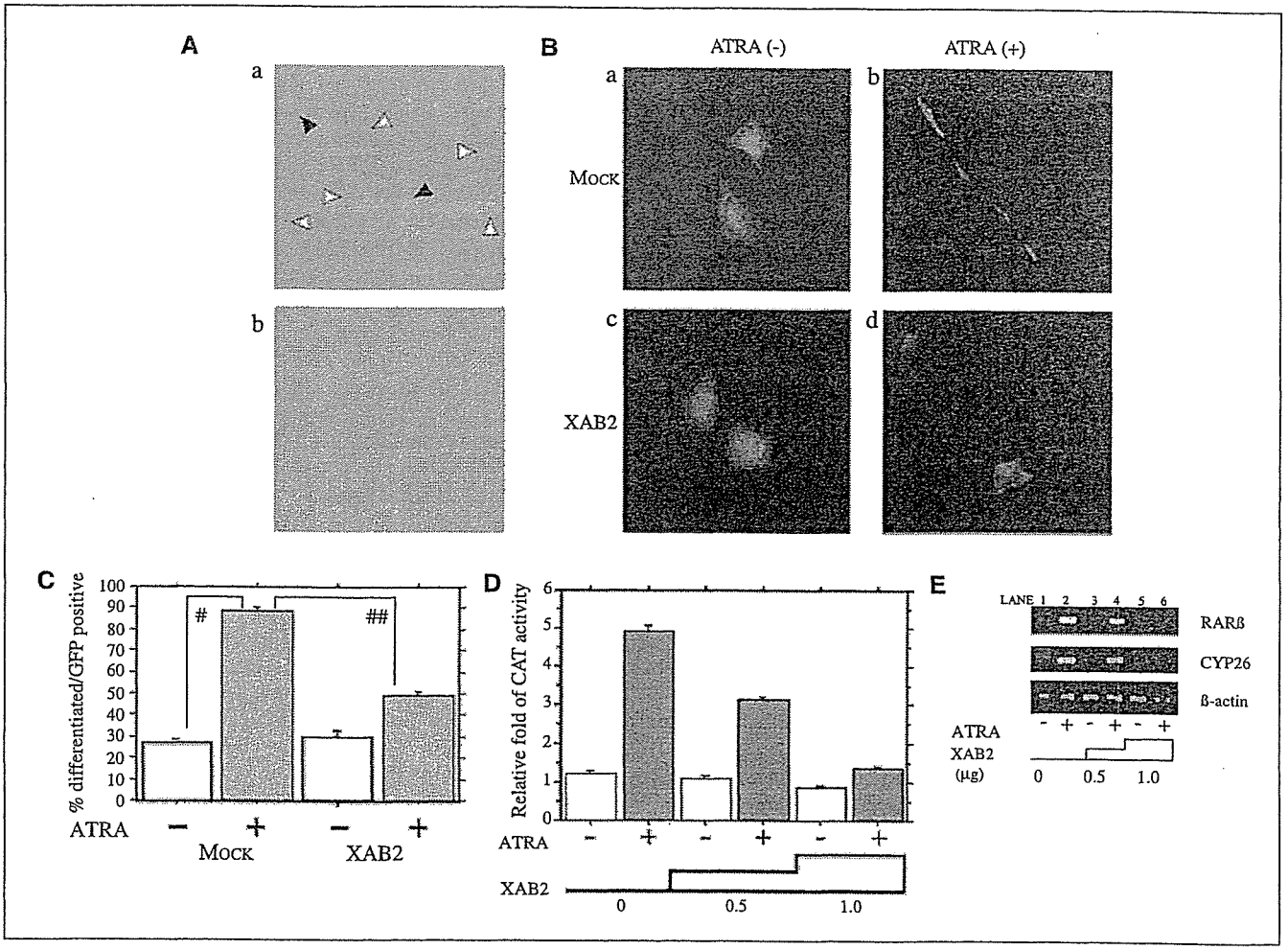

Figure 1. XAB2 inhibits ATRA-induced cellular differentiation and transcriptional activation. *A*, ATRA-sensitive human rhabdomyosarcoma MM-1-19-P cells were transiently transfected with pcDNA3 as a vector control (*a*) or pcDNA-XAB2 (*b*). Twelve hours later, the transfection medium was replaced with fresh media containing 2 μmol/L ATRA. After 24-h incubation, cells were visualized with phase-contrast microscopy. *Black* and *white arrowheads*, differentiated cells that form myotube-like processes. *B*, MM-1-19-P cells were transfected with 2 μg of pcDNA3 (*a* and *b*) or pcDNA3-XAB2 (*c* and *d*) and cotransfected with 0.4 μg of pEGFP-C1 to identify transfected cells (*a–d*). Cells were treated with DMSO vehicle as a control (*a* and *c*) or with ATRA (*b* and *d*) by the same method as described in (*A*) and visualized by fluorescence microscopy. Because the amount of pcDNA3-XAB2 transfected is five times more than that of pEGFP-C1, GFP-positive cells definitely contains exogenous XAB2. *C*, percentage of morphologically differentiated GFP-positive cells among 1,000 GFP-positive cells as shown in (*A*) and (*B*). *Columns*, mean from three independent experiments; *bars*, SE. # and ##, significant changes compared with control ($P < 0.05$). *D*, HepG2 cells were transiently transfected with pRARE-CAT (2 μg), pSV-β-gal (0.4 μg), and pcDNA3-XAB2 (0, 0.5, or 1.0 μg). The amount of expression vector was adjusted to 1 μg of pcDNA3 empty vector in each transfection. Twenty-four hours after transfection, cells were treated with 100 nmol/L ATRA or DMSO vehicle as a control. Cells were then harvested after 24 h and assayed for β-galactosidase and CAT activity. For transfection efficiency, CAT activity was normalized to β-galactosidase activity. The CAT activity in control cells treated with DMSO vehicle and a mock vector was set as equal to one and all other values are expressed as fold induction. *Columns*, mean from triplicate experiments; *bars*, SE. *E*, HEK293T cells were transiently transfected with pcDNA3 empty or pcDNA3-XAB2 vector (0, 0.5, or 1.0 μg). The amount of expression vector was adjusted to 1 μg of pcDNA3 empty vector in each transfection. Twenty-four hours after transfection, cells were treated with 1 μmol/L ATRA or DMSO vehicle as a control. Cells were then harvested after 24 h and total RNA was extracted. RT-PCR assays using primers for RARβ, CYP26, and β-actin (as internal control) were then done. All experiments were done at least thrice with similar results.

observed in HL60 cells treated with control siRNA. These data suggest that specific knockdown of XAB2 enhances ATRA-induced cellular differentiation at physiologic levels (10^{-9}–10^{-8} mol/L) as well as at therapeutic levels (10^{-7} mol/L).

To further confirm whether knockdown of XAB2 enhances ATRA-induced gene expression, we analyzed ATRA-targeted gene expression pattern in HL60 cells by RT-PCR, in the presence or absence of siRNA against XAB2. As shown in Fig. 2*C*, ATRA-induced mRNA expression of RARβ and CYP26 was increased in a dose-dependent manner (*lanes 1, 4, 7*, and *10*). The increased expression of RARβ and CYP26 mRNA was further enhanced in HL60 cells treated with siRNA against XAB2 (Fig. 2*C*, *lane 4* versus *lanes 5* and *6*, *lane 7* versus *lanes 8* and *9*, and *lane 10* versus *lanes 11* and *12*). This enhanced expression of RARβ and CYP26 mRNA was again observed to be dependent on ATRA doses (Fig. 2*C*, *lanes 5* and *6, 8* and *9*, and *11* and *12*). These data suggest that specific knockdown of XAB2 enhances not only cellular differentiation but also induction of ATRA-targeted genes at physiologic (10^{-9}–10^{-8} mol/L) and therapeutic (10^{-7} mol/L) levels.

XAB2 is associated with HDAC3. Retinoid-dependent cellular differentiation of embryonal carcinoma cell lines was previously shown to be mediated by HDAC activity (12, 15, 50). We thus examined whether XAB2 involvement in retinoid mediated-transcriptional regulation is through HDAC activity. For this purpose, the potential association of XAB2 with HDAC activity on RAR-regulated transcription was examined via RARE-chloramphenicol acetyltransferase (CAT) assays, which were done on the RAR reporter plasmid containing a RARE under the control of

thymidine kinase minimal promoter (pRARE-CAT). HepG2 cells were transiently transfected with pcDNA3-XAB2 to allow for the constitutive expression of XAB2 and were then grown in the presence or absence of ATRA. As shown in Fig. 3*A*, transcriptional activity was significantly enhanced by ATRA addition (Fig. 3*A*, #), and this ATRA-induced transcriptional activity was decreased in the presence of overexpression of XAB2 (Fig. 3*A*, ##). Moreover, the addition of trichostatin A or sodium butyrate, specific inhibitors of HDAC, completely antagonized the repression by XAB2 of RAR reporter activity (Fig. 3*A*, ###). To further confirm the antagonistic effect of HDAC inhibitors on XAB2-mediated repression, we analyzed the expression level of endogenous retinoic acid–targeted genes *RARβ* and *CYP26*. As shown in Fig. 3*B*, the mRNA level of RARβ and CYP26 was enhanced by ATRA addition (*lane 2*), and this ATRA-induced enhancement of RARβ and CYP26 mRNA expression was decreased by XAB2 overexpression (*lane 3*). In contrast, the addition of trichostatin A or sodium butyrate completely antagonized the repression by XAB2 of ATRA-induced RARβ and CYP26 mRNA expression (Fig. 3*B*, *lanes 4* and *5*).

These data suggest that the XAB2-mediated inhibitory effect of ATRA-induced transcriptional activity is associated with HDAC activity.

To further explore XAB2 association with HDACs, we next evaluated the potential interaction of XAB2 with HDACs in a transcriptional component through coimmunoprecipitation assays. HEK293T cells were transfected with an expression plasmid of GFP-XAB2 alone or together with expression plasmids of Flag-HDAC1, HDAC3, HDAC4, and HDAC6 (Fig. 3*C*, *top*). The Flag-HDACs were immunoprecipitated with antibody against the Flag tag, and coimmunoprecipitated GFP-XAB2 protein was detected by Western blotting with anti-GFP antibody. As shown in Fig. 3*C*, the GFP-XAB2 protein was coimmunoprecipitated with Flag-HDAC1, HDAC3, HDAC4, and HDAC6 from HEK293T cell lysates (*middle, lanes 1* and *3–5*). No cellular protein was detected by the anti-GFP antibody in immunoprecipitants of lysates of HEK293T cells transfected with Flag-vector control plasmid (*middle, lane 2*). The expression level of GFP-XAB2 was not affected by the presence or absence of Flag-HDACs (Fig. 3*C*, *bottom*).

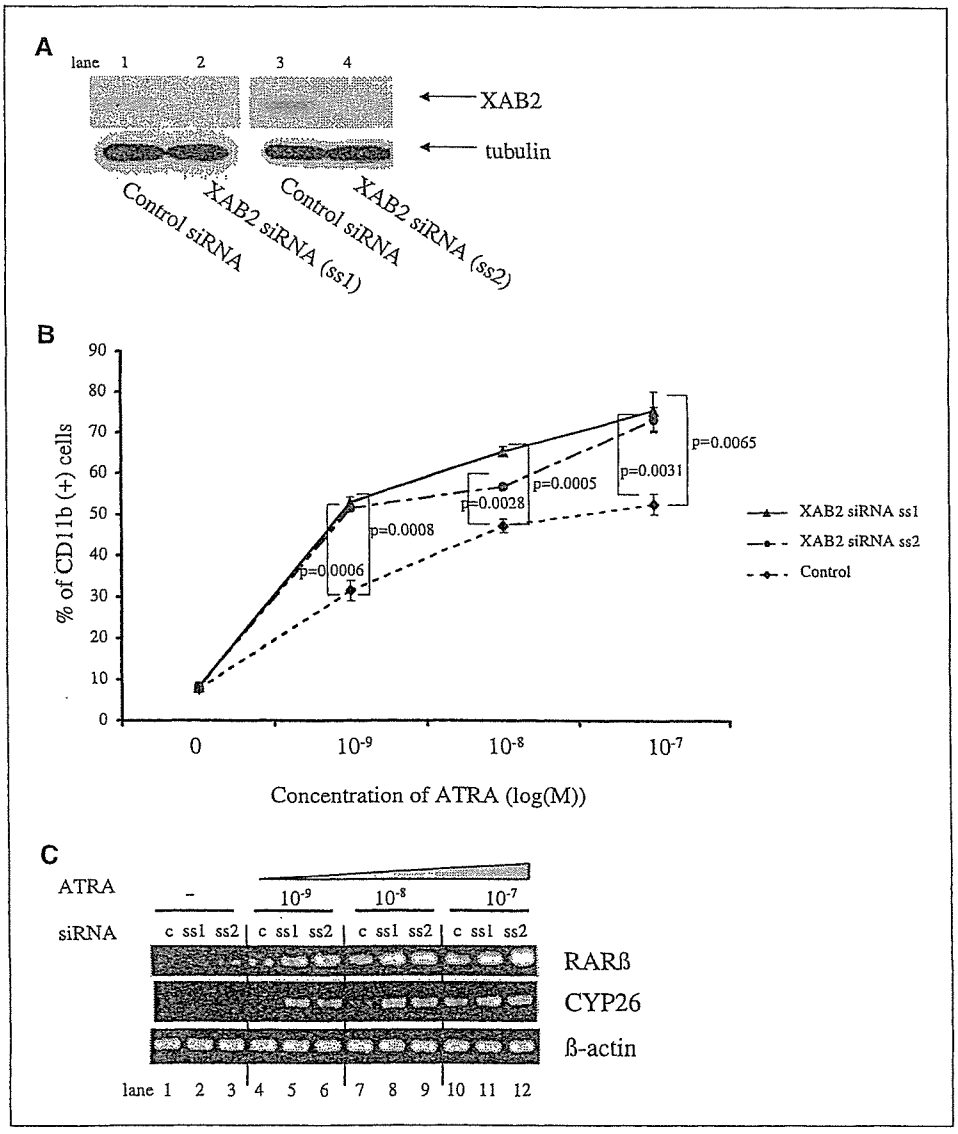

Figure 2. Knockdown of XAB2 by siRNA enhances ATRA-mediated cellular differentiation of HL60 cells. *A*, HL60 cells were transfected with sense siRNAs of *XAB2* gene (*XAB2 siRNA ss1* or *ss2*) or with control nonsense siRNA (*Control siRNA*) using Nucleofector. Cell lysates were resolved by 10% SDS-PAGE and immunoblotted with anti-XAB2 mAb, followed by stripping and reprobing with antitubulin mAb. All experiments were done at least thrice with similar results. *B*, effect of siRNAs against XAB2 on the induction of HL60 cell differentiation by ATRA. Following transfection with siRNA (XAB2 siRNA ss1, ss2, or control siRNA), HL60 cells were treated with ATRA at the indicated concentrations and incubated for 24 h. CD11b expression was analyzed by flow cytometry as described in Materials and Methods. *Points*, mean values calculated from three independent experiments; *bars*, SE. Percent values were percent of CD11b-positive cell number in 7-amino-actinomycin D–negative viable cells. *C*, following transfection with siRNA (XAB2 siRNA ss1, ss2, or control siRNA), HL60 cells were treated with ATRA at the indicated concentrations, or with DMSO vehicle as a control, and incubated for 24 h. Total RNA was extracted and RT-PCR assays using primers for RARβ, CYP26, and β-actin (as internal control) were then done. All experiments were done at least thrice with similar results.

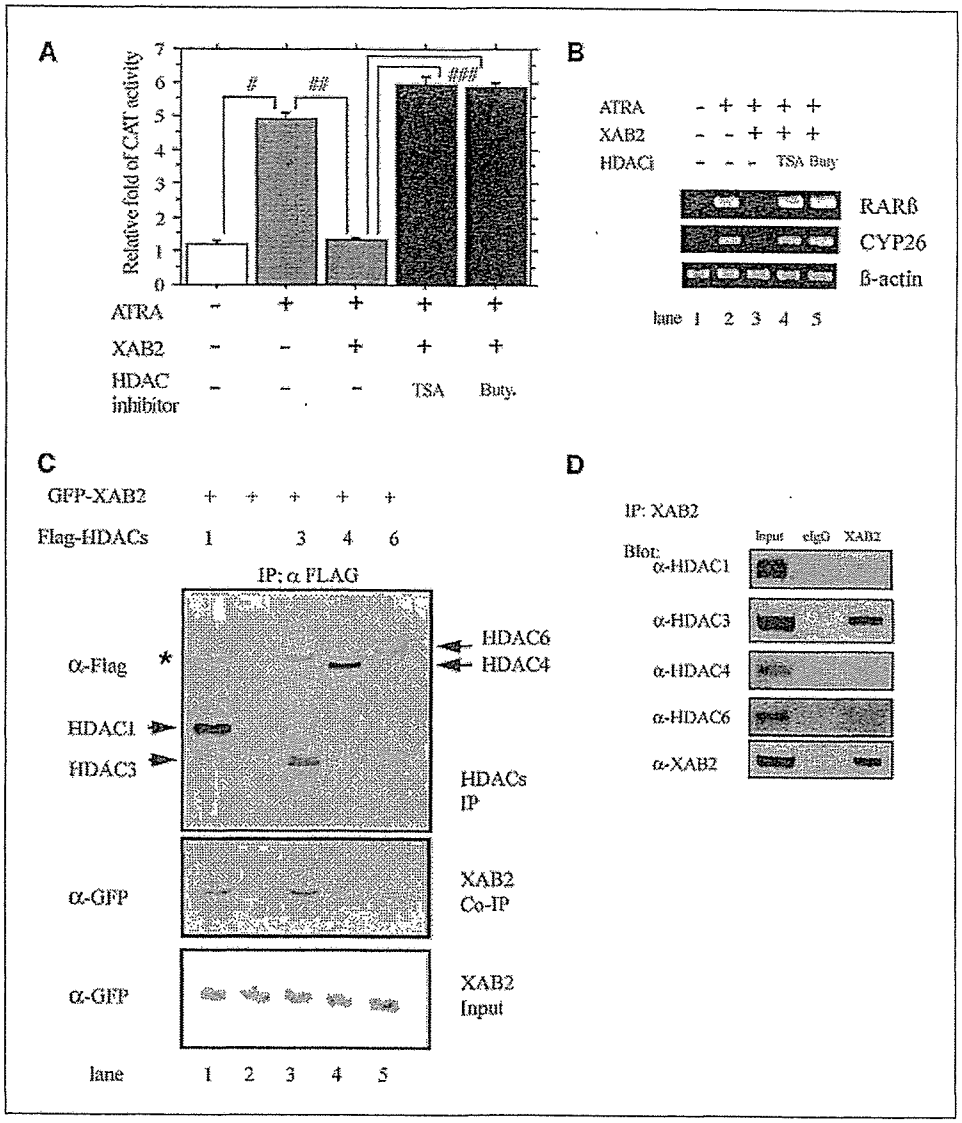

Figure 3. XAB2 is associated with HDAC3. *A*, HepG2 cells were transiently transfected with pRARE-CAT (2 μg), pSV-β-gal (0.4 μg), and pcDNA3-XAB2 (1.0 μg) or pcDNA3 empty vector (1.0 μg). Twenty-four hours after transfection, cells were treated with 100 nmol/L ATRA or DMSO vehicle as a control in the presence or absence of trichostatin A (*TSA*; 10 nmol/L) or sodium butyrate (*Buty*; 1 mmol/L). Cells were then harvested after 24 h and assayed for β-galactosidase and CAT activity. For transfection efficiency, CAT activity was normalized to β-galactosidase activity. CAT activity in control cells treated with DMSO vehicle and a mock vector was set as equal to one and all other values are expressed as fold induction. *Columns*, mean from triplicate experiments; *bars*, SE. #, ##, and ###, significant changes compared with control ($P < 0.05$). *B*, HEK293T cells were transiently transfected with pcDNA3 empty or pcDNA3-XAB2 vector (1.0 μg). Twenty-four hours after transfection, cells were treated with 1 μmol/L ATRA or DMSO vehicle as a control in the presence or absence of trichostatin A (10 nmol/L) or sodium butyrate (1 mmol/L). Cells were then harvested after 24 h and total RNA was extracted. RT-PCR assays using primers for RARβ, CYP26, and β-actin (as internal control) were then done. All experiments were done at least thrice with similar results. *C*, HEK293T cells were transfected with pEGFP-C1-XAB2 and pFLAG-CMV-HDACs (*lane 1*, HDAC1; *lane 3*, HDAC3; *lane 4*, HDAC4; *lane 5*, HDAC6). pFLAG-CMV empty vector was transfected along with pEGFP-C1-XAB2 (*lane 2*). After 24-h transfection, cells were harvested and nuclear extracts were immunoprecipitated with anti-Flag M2 mAb and then Western blotted with anti-Flag M2 mAb (*top*) or anti-GFP polyclonal antibody (*middle*). Ten micrograms of nuclear extracts were Western blotted with anti-GFP polyclonal antibody to show equal expression of transfected GFP-XAB2 protein (*bottom*). *Asterisk*, nonspecific bands. *D*, in the absence of ATRA, nuclear extracts were prepared from HL60 cells and immunoprecipitation (*IP*) assays were conducted with anti-XAB2 antibody or control immunoglobulin (*cIgG*). Immunoprecipitation complexes, along with 10% input of nuclear extract, were then separated by 4% to 20% SDS-PAGE, followed by Western blotting with indicated antibodies. Representative results obtained from three independent experiments.

Various HDACs have previously been reported to be involved in RARα-mediated transcriptional regulation via interaction with N-CoR/SMRT (20, 51, 52). However, the identity of the precise HDACs involved remains controversial, partly because of the different cell types or assay systems being used. We therefore attempted to determine the specific HDACs among HDAC1, HDAC3, HDAC4, or HDAC6 that are associated with XAB2 in our system. For this purpose, immunoprecipitation assays detecting endogenous HDACs and XAB2 proteins were done on nuclear extract of HL60 cells. As shown in Fig. 3*D*, endogenous HDAC1, HDAC3, HDAC4, HDAC6, and XAB2 were expressed in HL60 cells (*lane 1*), with each control immunoglobulin G (IgG) not able to precipitate endogenous HDAC1, HDAC3, HDAC4, HDAC6, and XAB2 (*lane 2*). In this experimental system, HDAC3 was clearly detected in the complex precipitated by XAB2 whereas very slight amount of HDAC1 was coprecipitated with XAB2. On the other hand, no portion of HDAC4 or HDAC6 was detected in the complex (*lane 2*). These data indicate that XAB2 is associated mainly with

HDAC3 in our system and that XAB2 associates with HDAC3-dependent transcriptional components that interact with RARE.

ATRA leads to dissociation of XAB2 from RARα and HDAC3. As shown above, XAB2 is associated mostly with HDAC3 and is involved in the suppression of ATRA-mediated cellular differentiation. We next examined potential alterations in the complex containing endogenous XAB2, RARα, and HDAC3 after ATRA treatment. For this purpose, we conducted immunoprecipitation experiments using nuclear extracts of HL60 cells incubated in the presence or absence of ATRA. As shown in Fig. 4*A*, XAB2 was found with RARα and HDAC3 in immunoprecipitation complexes of nuclear extracts of untreated cells (Fig. 4*A*, *lanes 1* and *4*). Following treatment of HL60 cells with ATRA for 24 to 72 h, XAB2 and HDAC3 were dissociated from RARα (Fig. 4*A*, *lanes 2* and *3*) and, similarly, RARα and HDAC3 were dissociated from XAB2 (Fig. 4*A*, *lanes 5* and *6*). At these time points, Western blot analysis of nuclear extracts revealed that the expression level of HDAC3 was decreased by ATRA treatment (Fig. 4*B*, *middle*), whereas the expression levels of XAB2 and tubulin were not changed. These data indicate that XAB2 forms a complex with RARα and HDAC3 and that, following ATRA treatment, XAB2 is disengaged from the complex without degradation while HDAC3 is degraded, as previously reported (22).

To further characterize the association among XAB2, HDAC3, and RARα, we did fluorescence microscopic analysis to determine the subcellular localization of these structures. As shown in Fig. 4*C*, XAB2 clearly colocalized with RARα, as well as HDAC3, in the nuclei of untreated HL60 cells (*a–c* and *g–i*). Following treatment of HL60 cells with ATRA, XAB2 was not found to colocalize with RARα (*d–f*). Moreover, whereas XAB2 was localized in the nuclei after ATRA treatment (*e* and *j*), HDAC3 was not detected in the nuclei after ATRA treatment (*k*). Taken together, these data indicate that XAB2 associates with HDAC3 and RARα in the nuclei of untreated HL60 cells, with ATRA treatment resulting in the subsequent disengagement of XAB2 and HDAC3 from the complex. Furthermore, ATRA treatment induces change of localization of XAB2 in the nuclei while HDAC3 is degraded as reported previously (22).

To further confirm that XAB2, RARα, and HDAC3 bind to the same ATRA-targeted gene promoters and that XAB2 and HDAC3

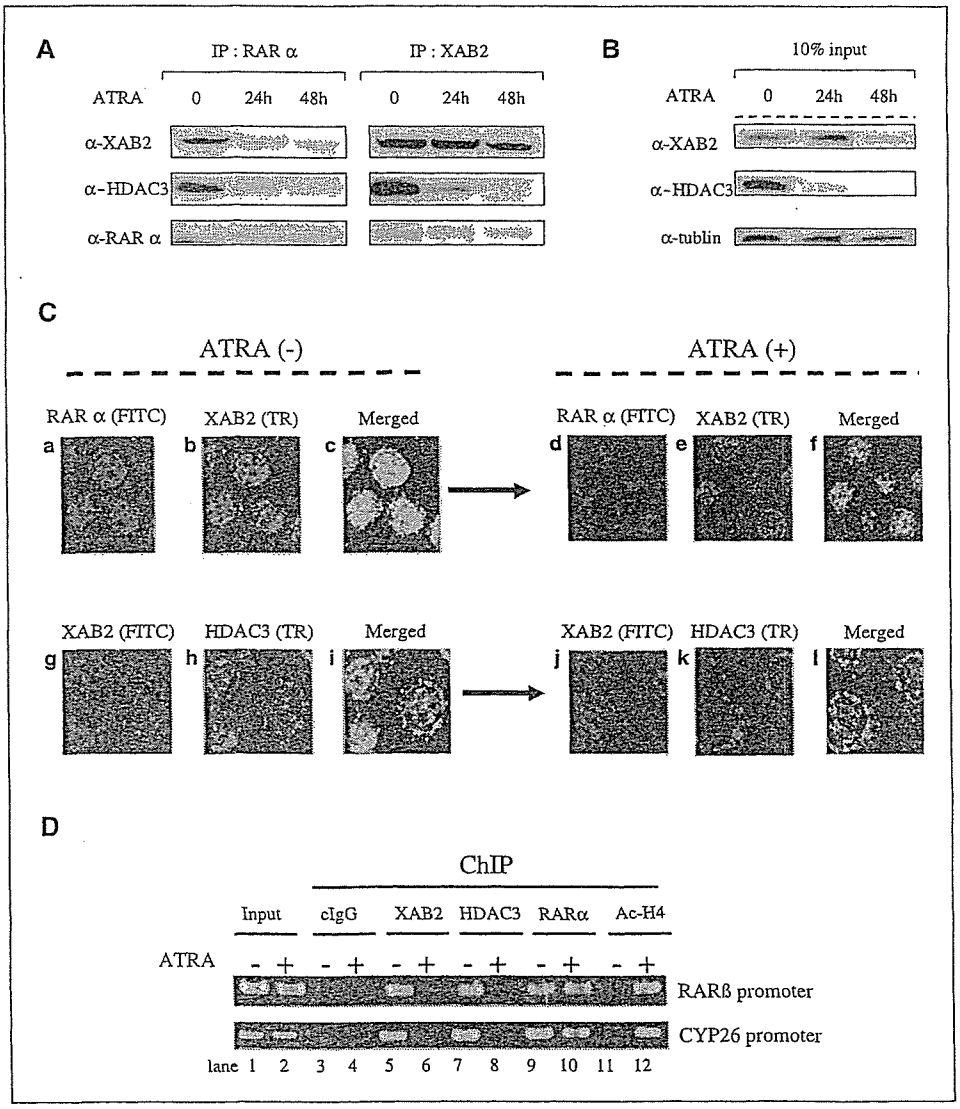

Figure 4. XAB2 forms a complex with RARα and HDAC3 and is dissociated from the complex following ATRA treatment. *A*, nuclear extracts of HL60 cells were immunoprecipitated with anti-RARα polyclonal antibody or anti-XAB2 mAb in the presence of absence of ATRA treatment (24 or 48 h) and Western blotted with anti-XAB2 mAb, anti-HDAC3 polyclonal antibody, or anti-RARα polyclonal antibody. *B*, 10 μg of nuclear extracts of HL60 cells were Western blotted with anti-XAB2 mAb, anti-HDAC3 polyclonal antibody, or antitubulin mAb in the presence of absence of ATRA treatment (24 or 48 h). *C*, HL60 cells were treated with ATRA (1 μmol/L) or DMSO vehicle for 24 h and submitted to analysis using confocal laser microscopy as described in Materials and Methods. *D*, chromatin immunoprecipitation assay was done using HL60 cells treated with ATRA (1 μmol/L) or DMSO vehicle for 24 h. Extracted chromatin samples were used directly in the PCR for the input control (*lanes 1* and *2*). Goat polyclonal IgG was used as negative control (*cIgG*; *lanes 3* and *4*). Antibodies for XAB2 (*lanes 5* and *6*), HDAC3 (*lanes 7* and *8*), RARα (*lanes 9* and *10*), and acetylated histone H4 (*Ac-H4*; *lanes 11* and *12*) were used for immunoprecipitation of the endogenous proteins. PCR was done using primers for RARβ and CYP26 promoters containing RARE as described in Materials and Methods. All experiments were done at least thrice with similar results.

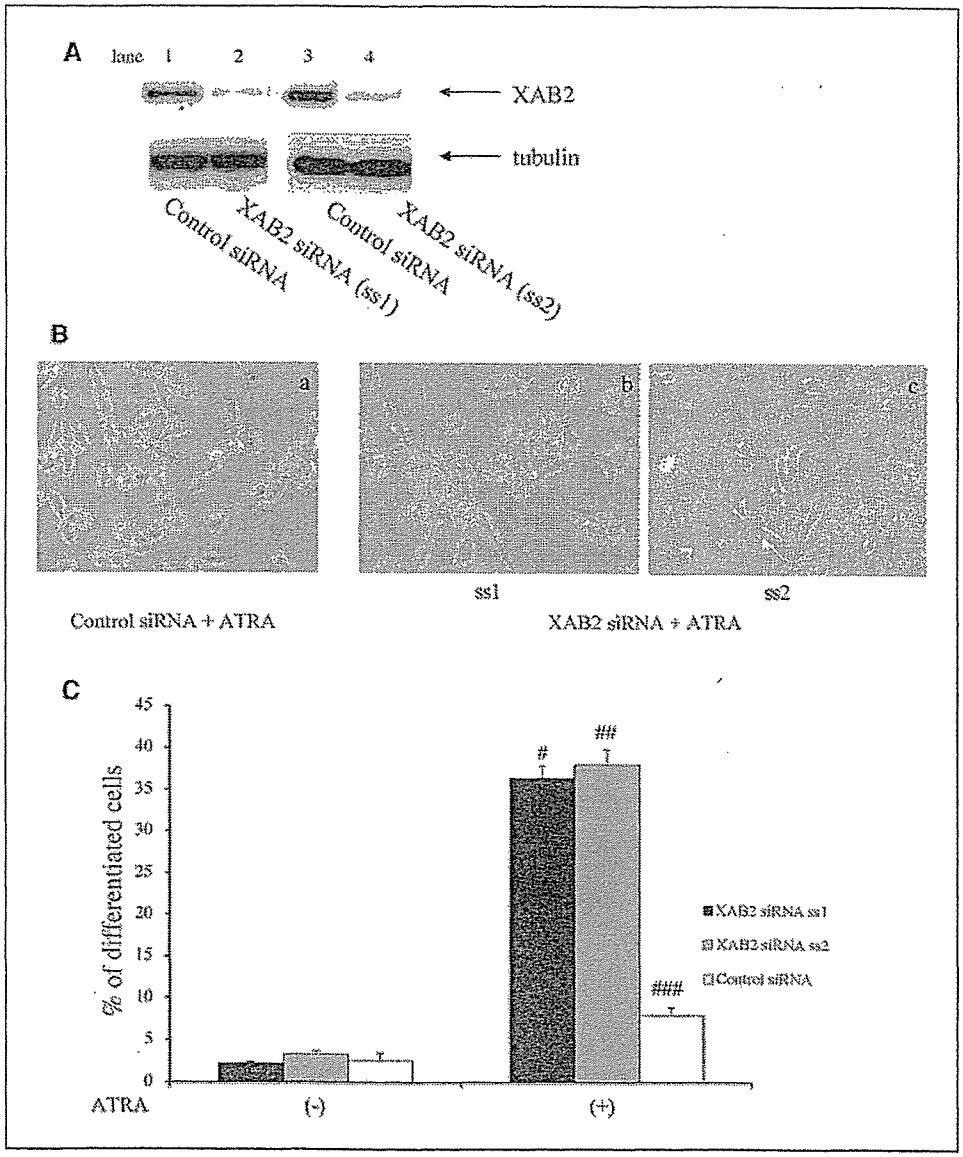

Figure 5. Knockdown of XAB2 by siRNA enhances ATRA-mediated cellular differentiation of ATRA-resistant neuroblastoma cells. *A*, ATRA-resistant neuroblastoma cell line IMR-32 was transfected with sense siRNAs of *XAB2* gene (XAB2 siRNA ss1 or ss2) or with control nonsense siRNA using Nucleofector. Cell lysates were resolved by 10% SDS-PAGE and immunoblotted with anti-XAB2 mAb, followed by stripping and reprobing with antitubulin mAb. All experiments were done at least thrice with similar results. *B*, effect of siRNA against XAB2 on ATRA-induced IMR-32 cell differentiation. After 48 h of transfection with siRNA (XAB2 siRNA ss1, ss2, or control siRNA), IMR-32 cells (1×10^6/mL) were treated with 2 μmol/L ATRA for an additional 24 h and photographed using phase-contrast microscopy. *C*, IMR-32 cells were treated with the same method as described in (*B*). Cells extending processes longer than twice the diameter of the cell body were counted as being differentiated, and two pathologists identified the morphologic changes to formation of neurite-like processes. The graph shows the percentage of differentiated cells among 1,000 quantified cells. *Columns*, mean of triplicate experiments; *bars*, SE. # and ##, significant changes compared with control ($P < 0.05$).

disengage from these genes following ATRA treatment, we did chromatin immunoprecipitation assay with HL60 cells. For this purpose, HL60 cells were treated in the presence or absence of ATRA for 24 h, followed by cross-linking by formaldehyde, and chromatin-protein complexes were immunoprecipitated using control IgG, anti-XAB2 pAb, anti-HDAC3 pAb, anti-RARα pAb, or anti–acetyl-histone H4 pAb. Chromatin immunoprecipitation assays against endogenous RARβ and CYP26 promoters that contain RARE sequences were done (47). As shown in Fig. 4*D*, endogenous XAB2 and HDAC3 were recruited to RARβ and CYP26 promoters in the absence of ATRA (*lanes 5* and *7*). However, in the presence of ATRA, endogenous XAB2 and HDAC3 were released from RARβ and CYP26 promoters (Fig. 4*D*, *lanes 6* and *8*). On the other hand, endogenous RARα bound to RARβ and CYP26 promoters constitutively in the presence or absence of ATRA (Fig. 4*D*, *lanes 9* and *10*). Moreover, to determine the acetylation level of histones around the RARE region of *RARβ* and *CYP26* genes, chromatin immunoprecipitation assays with anti–acetylated histone H4 pAb were done. In the absence of ATRA, histone acetylation levels of RARβ and CYP26 promoters were decreased (Fig. 4*D*, *lane 11*). On the other hand, in the presence of ATRA, histone acetylation level of these promoters was significantly increased (Fig. 4*D*, *lane 12*). These data suggest that XAB2 forms a complex with RARα and HDAC3 on the same ATRA-targeted genes and that, following ATRA treatment, XAB2 and HDAC3 are disengaged from the complex, which is associated with increased level of promoter histone acetylation.

Knockdown of XAB2 by siRNA induces differentiation of ATRA-resistant neuroblastoma cell line. In view of XAB2 inhibitory effect on ATRA-mediated transcriptional activity and cellular differentiation, we examined the effect of XAB2 on ATRA-mediated cellular differentiation of ATRA-resistant cells. For this purpose, we conducted siRNA experiments using the ATRA-resistant human neuroblastoma cell line IMR-32 (53). We prepared two specific siRNAs against XAB2 as described in Materials and Methods, which effectively knocked down XAB2 expression in IMR-32 cells (Fig. 5*A*, *top*, *lanes 2* and *4*). Because XAB2 in IMR-32 cells was not significantly knocked down by control siRNA (Fig. 5*A*, *top*, *lanes 1* and *3*) and expression level of tubulin as a housekeeping protein was not affected by both siRNAs (Fig. 5*A*, *bottom*), the

observed inhibition of XAB2 expression by its siRNA was specific. In addition, the expression levels of RARα and HDAC3 were not altered by treatment of XAB2-specific siRNA (data not shown). We next examined the effect of ATRA on cell differentiation of IMR-32 cells with XAB2 expression being knocked down by siRNA. As shown in Fig. 5*B*, changes consistent with cell differentiation following treatment with ATRA were not observed in ATRA-resistant IMR-32 cells treated with control siRNA (*a*). On the other hand, ATRA-resistant IMR-32 cells treated with two separate siRNAs against XAB2 exhibited ATRA-induced cell differentiation (*b* and *c*). Quantification of cell differentiation by ATRA in IMR-32 cells is shown in Fig. 5*C*. As shown in microscopic observation study (Fig. 5*B*, *a–c*), neurite-like differentiation of ATRA-resistant IMR-32 induced by ATRA treatment was significantly increased in cells treated with siRNAs against XAB2 (Fig. 5*C*, # and ##) compared with cell treated with control siRNA (Fig. 5*C*, ###). Although the precise mechanisms of ATRA resistance in IMR-32 have not yet been revealed (53), these data suggest that XAB plays an inhibitory role in ATRA-induced cell differentiation and that knockdown of XAB2 in selected ATRA-resistant tumors induces ATRA-mediated cellular differentiation.

Discussion

In this study, we showed that overexpression of XAB2 inhibited ATRA-induced cellular differentiation of the human rhabdomyosarcoma cell line MM-1-19-P and that knockdown of XAB2 by siRNA enhanced ATRA-mediated cellular differentiation of the human promyelocytic leukemia cell line HL60. Moreover, we found that XAB2 was associated with RARα and HDAC3 in the nuclei. Finally, we showed that, following treatment with siRNA specific against XAB2, the ATRA-resistant neuroblastoma cell line IMR-32 underwent cellular differentiation when incubated with ATRA at a therapeutic concentration.

XAB2 has been isolated by virtue of its ability to interact with XPA in the yeast two-hybrid system (33). Xeroderma pigmentosum patients show striking hypersensitivity to sunlight and an extremely high incidence of skin cancer in sun-exposed areas, as well as frequently progressive neurologic degeneration (40). Antibodies against the XAB2 protein has been shown to inhibit transcription in non–UV-irradiated normal cells, strongly suggesting that XAB2 can be a novel factor involved in the transcription process itself. In addition, it has previously been shown that retinoids are effective in treating preneoplastic diseases including xeroderma pigmentosum and other dermatologic diseases such as photoaging. We thus aimed to analyze the effect of XAB2 on retinoid-mediated transcription in the present study, especially on ATRA-mediated cellular differentiation, as cancer therapy. Our *in vitro* analyses shown in Figs. 1 and 2 showed that XAB2 has an inhibitory effect on ATRA-induced cellular differentiation of ATRA-sensitive neoplastic cell lines and that ATRA-mediated transcriptional activity is inhibited by XAB2 in a dose-dependent manner. Moreover, expression levels of endogenous RARα and HDAC3 are not affected by overexpression of exogenous XAB2 or by knockdown of XAB2 by siRNA (Figs. 2, 3, and 5). These results suggest that XAB2 plays an inhibitory role in ATRA-induced cellular differentiation by being functionally associated with the transcriptional repressor complex existing in RARE.

Our next focus in this study was to analyze the molecular mechanisms of XAB2-mediated inhibitory effect on ATRA-induced cellular differentiation. As shown in Figs. 3 and 4, XAB2 forms a complex with RARα and HDAC3 and is dissociated from RARα and HDAC3 in the presence of ATRA treatment. In the absence of ligands for RAR-RXR dimers such as ATRA, genes targeted by the receptors are repressed (reviewed in ref. 3). This is due to the recruitment of HDAC-containing complexes that are tethered through corepressors, such as N-CoR/SMRT, to the nonliganded RAR-RXR dimers. Moreover, the repressive activity of the N-CoR/SMRT complex results from direct or indirect association with HDAC3, leading to the formation of a stoichiometric core complex with N-CoR/SMRT (24, 54). Our data shown in Figs. 3 and 4 suggest that XAB2 is associated with corepressor complexes that bind to RARα and/or HDAC3 to repress transcriptional activity in the absence of ATRA. On the other hand, on binding of ligands to RAR, the corepressor interface is destabilized to generate a novel interaction surface for coactivators such as histone acetyltransferases and cAMP-responsive element binding protein–binding proteins or p300, leading to transcription initiation (3). To switch from corepressors to coactivators following ligand binding to RARα-RXR, specific adaptors are required for dismissal and subsequent degradation by ubiquitination of corepressors N-CoR/SMRT/HDAC3 (22, 24). TBL1/TBLR1 has been reported to serve as specific adaptors for the recruitment of the ubiquitin-conjugating proteosome complex to degrade N-CoR/SMRT/HDAC3 (55). In this

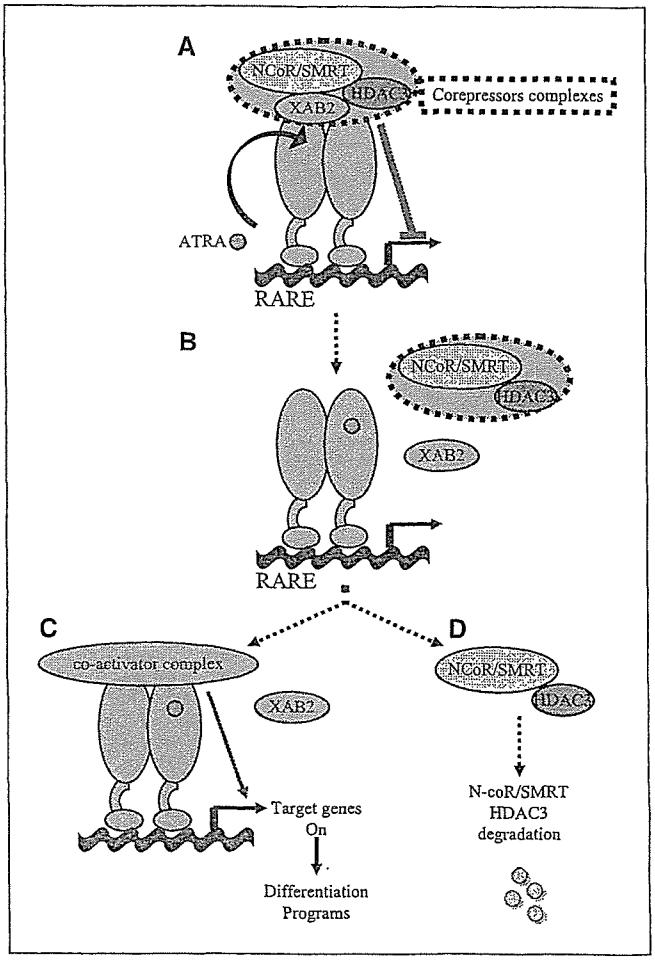

Figure 6. Model for the molecular interaction of XAB2 with RARα/RXR and N-CoR/SMRT corepressor complexes. See text for details.

regard, although it is presently unclear whether XAB2 is degraded or recycled via an unknown pathway, XAB2 remains localized in the nuclei after ATRA treatment (Fig. 4) while still disengaging a corepressor complex containing N-CoR/SMRT, HDAC3, and XAB2 from RARα-RXR on RARE (Fig. 4), potentially mediating corepressor/coactivator exchange.

Our findings suggest XAB2 interaction with corepressor complex containing HDAC3 and RARα through biochemical assays revealing protein-protein association and cellular assays showing biological effects (Figs. 3 and 4). However, our data also raise questions about the functional implication of XAB2 binding to HDAC3 and RARα. As shown in Fig. 3, endogenous XAB2 was mainly associated with HDAC3, whereas a small amount of HDAC1 was coprecipitated with XAB2. In fact, the precise mechanism of HDACs involvement in retinoid signaling is controversial (56). We therefore could not exclude the possibility that HDAC1 is involved in XAB2-associated retinoid signaling, a topic which will be elucidated in future studies. Another issue raised by our findings is whether XAB2 is involved in other nuclear receptor systems than RARα, such as vitamin D receptor or thyroid hormone receptor (24). Indeed, corepressor complex such as N-CoR/SMRT/HDACs also regulates other nuclear receptor systems than RARα (19), suggesting that XAB2 may be possibly involved in other transcriptional systems. Whereas data shown in our present study were obtained in transient transfection systems, we plan to examine the inhibitory effect of XAB2 on retinoid signaling or other nuclear receptor systems with stably transfected systems of overexpression and siRNAs in future studies.

On the basis of our results, we propose a model to describe the role of XAB2 in cell responsiveness to retinoids (Fig. 6). In this model, unliganded RARα-RXR heterodimers bind to RARE and recruit HDAC3 complexes containing XAB2, followed by suppression of target genes for differentiation blockade (Fig. 6, *a*). On binding of ligands such as ATRA to RARα, N-CoR/SMRT/HDAC3 corepressors are dismissed and subsequently degraded by ubiquitination, which is mediated by specific adaptors such as TBL1/TBLR1 (Fig. 6, *b* and *c*). Subsequently, coactivator complexes such as cAMP-responsive element binding protein–binding protein or p300 are recruited, leading to target gene activation and differentiation programs (Fig. 6, *d*). The potential clinical relevance of this model is revealed by the fact that pharmacologic concentrations of ATRA are required in the presence of XAB2 to disrupt this complex. However, combining ATRA treatment with knockdown of XAB2 by siRNA allows for the dissociation of the repressor complex containing HDAC3 and XAB2, leading subsequently to cellular differentiation.

Work over the past decades has shown that retinoids and their cognate receptors are required for the proper functioning of a number of organs, including the skin, and of the neuronal system and for prevention and treatment of selected cancers (17, 57, 58). One of the important objectives of cancer differentiation therapy is to selectively induce growth inhibition through RAR-dependent pathways. Our findings therefore should have broad implications for potential therapy not only for ATRA-sensitive cancer such as acute promyelocytic leukemia and rhabdomyosarcoma but also for ATRA-resistant solid tumors including neuroblastoma.

Acknowledgments

Received 5/11/2006; revised 10/24/2006; accepted 11/20/2006.

Grant support: Japan Leukemia Research Fund (K. Ohnuma-Ishikawa) and Grant-in-Aid of Ministry of Education, Science, Sports, and Culture and Ministry of Health, Labor, and Welfare, Japan (S. Mizutani, K. Ohnuma, and C. Morimoto).

The costs of publication of this article were defrayed in part by the payment of page charges. This article must therefore be hereby marked *advertisement* in accordance with 18 U.S.C. Section 1734 solely to indicate this fact.

We thank Yuko Kutami for her technical assistance.

References

1. Lotan R. Retinoids in cancer chemoprevention. FASEB J 1996;10:1031–9.
2. Freemantle SJ, Spinella MJ, Dmitrovsky E. Retinoids in cancer therapy and chemoprevention: promise meets resistance. Oncogene 2003;22:7305–15.
3. Altucci L, Gronemeyer H. The promise of retinoids to fight against cancer. Nat Rev Cancer 2001; 1:181–93.
4. Hong WK, Sporn MB. Recent advances in chemoprevention of cancer. Science 1997;278:1073–7.
5. Sun SY, Lotan R. Retinoids and their receptors in cancer development and chemoprevention. Crit Rev Oncol Hematol 2002;41:41–55.
6. Thacher SM, Vasudevan J, Chandraratna RA. Therapeutic applications for ligands of retinoid receptors. Curr Pharm Des 2000;6:25–58.
7. Huang ME, Ye YC, Chen SR, et al. Use of all-*trans* retinoic acid in the treatment of acute promyelocytic leukemia. Blood 1988;72:567–72.
8. Tallman MS, Andersen JW, Schiffer CA, et al. All-*trans*-retinoic acid in acute promyelocytic leukemia. N Engl J Med 1997;337:1021–8.
9. de The H, Chomienne C, Lanotte M, Degos L, Dejean A. The t(15;17) translocation of acute promyelocytic leukaemia fuses the retinoic acid receptor α gene to a novel transcribed locus. Nature 1990;347:558–61.
10. Kakizuka A, Miller WH, Jr., Umesono K, et al. Chromosomal translocation t(15;17) in human acute promyelocytic leukemia fuses RARα with a novel putative transcription factor, PML. Cell 1991;66:663–74.
11. Piazza F, Gurrieri C, Pandolfi PP. The theory of APL. Oncogene 2001;20:7216–22.
12. Ferrara FF, Fazi F, Bianchini A, et al. Histone deacetylase-targeted treatment restores retinoic acid signaling and differentiation in acute myeloid leukemia. Cancer Res 2001;61:2–7.
13. Grignani F, De Matteis S, Nervi C, et al. Fusion proteins of the retinoic acid receptor-α recruit histone deacetylase in promyelocytic leukaemia. Nature 1998;391:815–8.
14. Lin RJ, Nagy L, Inoue S, Shao W, Miller WH, Jr., Evans RM. Role of the histone deacetylase complex in acute promyelocytic leukaemia. Nature 1998;391:811–4.
15. Warrell RP, Jr., He LZ, Richon V, Calleja E, Pandolfi PP. Therapeutic targeting of transcription in acute promyelocytic leukemia by use of an inhibitor of histone deacetylase. J Natl Cancer Inst 1998;90:1621–5.
16. Leid M, Kastner P, Lyons R, et al. Purification, cloning, and RXR identity of the HeLa cell factor with which RAR or TR heterodimerizes to bind target sequences efficiently. Cell 1992;68:377–95.
17. Chambon P. A decade of molecular biology of retinoic acid receptors. FASEB J 1996;10:940–54.
18. Urnov FD, Wolffe AP, Guschin D. Molecular mechanisms of corepressor function. Curr Top Microbiol Immunol 2001;254:1–33.
19. Chen JD, Evans RM. A transcriptional co-repressor that interacts with nuclear hormone receptors. Nature 1995;377:454–7.
20. Chen JD, Umesono K, Evans RM. SMRT isoforms mediate repression and anti-repression of nuclear receptor heterodimers. Proc Natl Acad Sci U S A 1996; 93:7567–71.
21. Xu L, Glass CK, Rosenfeld MG. Coactivator and corepressor complexes in nuclear receptor function. Curr Opin Genet Dev 1999;9:140–7.
22. Guenther MG, Barak O, Lazar MA. The SMRT and N-CoR corepressors are activating cofactors for histone deacetylase 3. Mol Cell Biol 2001;21:6091–101.
23. Wen YD, Perissi V, Staszewski LM, et al. The histone deacetylase-3 complex contains nuclear receptor corepressors. Proc Natl Acad Sci U S A 2000;97:7202–7.
24. Li J, Wang J, Wang J, et al. Both corepressor proteins SMRT and N-CoR exist in large protein complexes containing HDAC3. EMBO J 2000;19:4342–50.
25. Zhang J, Kalkum M, Chait BT, Roeder RG. The N-CoR-HDAC3 nuclear receptor corepressor complex inhibits the JNK pathway through the integral subunit GPS2. Mol Cell 2002;9:611–23.
26. Sternsdorf T, Phan VT, Maunakea ML, et al. Forced retinoic acid receptor α homodimers prime mice for APL-like leukemia. Cancer Cell 2006;9:81–94.
27. Kwok C, Zeisig BB, Dong S, So CW. Forced homooligomerization of RARα leads to transformation of primary hematopoietic cells. Cancer Cell 2006;9:95–108.
28. Coffey DC, Kutko MC, Glick RD, et al. Histone deacetylase inhibitors and retinoic acids inhibit growth of human neuroblastoma *in vitro*. Med Pediatr Oncol 2000;35:577–81.
29. Gottlicher M, Minucci S, Zhu P, et al. Valproic acid defines a novel class of HDAC inhibitors inducing differentiation of transformed cells. EMBO J 2001;20: 6969–78.
30. Marks PA, Richon VM, Rifkind RA. Histone deacetylase inhibitors: inducers of differentiation or apoptosis of transformed cells. J Natl Cancer Inst 2000;92: 1210–6.
31. Petti MC, Fazi F, Gentile M, et al. Complete remission through blast cell differentiation in PLZF/RARα-positive acute promyelocytic leukemia: *in vitro* and *in vivo* studies. Blood 2002;100:1065–7.
32. Zhou DC, Kim SH, Ding W, Schultz C, Warrell RP, Jr., Gallagher RE. Frequent mutations in the ligand-binding domain of PML-RARα after multiple relapses of acute

promyelocytic leukemia: analysis for functional relationship to response to all-*trans* retinoic acid and histone deacetylase inhibitors *in vitro* and *in vivo*. Blood 2002;99:1356–63.
33. Nakatsu Y, Asahina H, Citterio E, et al. XAB2, a novel tetratricopeptide repeat protein involved in transcription-coupled DNA repair and transcription. J Biol Chem 2000;275:34931–7.
34. Yonemasu R, Minami M, Nakatsu Y, et al. Disruption of mouse XAB2 gene involved in pre-mRNA splicing, transcription and transcription-coupled DNA repair results in preimplantation lethality. DNA Repair (Amst) 2005;4:479–91.
35. Fousteri M, Vermeulen W, van Zeeland AA, Mullenders LH. Cockayne syndrome A and B proteins differentially regulate recruitment of chromatin remodeling and repair factors to stalled RNA polymerase II *in vivo*. Mol Cell 2006;23:471–82.
36. Hoeijmakers JH. Genome maintenance mechanisms for preventing cancer. Nature 2001;411:366–74.
37. Lindahl T, Wood RD. Quality control by DNA repair. Science 1999;286:1897–905.
38. Berneburg M, Lehmann AR. Xeroderma pigmentosum and related disorders: defects in DNA repair and transcription. Adv Genet 2001;43:71–102.
39. Daya-Grosjean L, Sarasin A. The role of UV induced lesions in skin carcinogenesis: an overview of oncogene and tumor suppressor gene modifications in xeroderma pigmentosum skin tumors. Mutat Res 2005;571:43–56.
40. Lambert WC. Xeroderma pigmentosum. Neth J Med 1989;86:383–6.
41. Lehmann AR, Bridges BA. Sunlight-induced cancer: some new aspects and implications of the xeroderma pigmentosum model. Br J Dermatol 1990;122 Suppl 35: 115–9.
42. Ishii T, Ohnuma K, Murakami A, et al. SS-A/Ro52, an autoantigen involved in CD28-mediated IL-2 production. J Immunol 2003;170:3653–61.
43. Sandquist D, Williams TH, Sahu SK, Kataoka S. Morphological differentiation of a murine neuroblastoma clone in monolayer culture induced by dexamethasone. Exp Cell Res 1978;113:375–81.
44. Ohnuma K, Munakata Y, Ishii T, et al. Soluble CD26/dipeptidyl peptidase IV induces T cell proliferation through CD86 up-regulation on APCs. J Immunol 2001; 167:6745–55.
45. Ohnuma K, Yamochi T, Uchiyama M, et al. CD26 up-regulates expression of CD86 on antigen-presenting cells by means of caveolin-1. Proc Natl Acad Sci U S A 2004; 101:14186–91.
46. Hosoi H, Sugimoto T, Hayashi Y, et al. Differential expression of myogenic regulatory genes, MyoD1 and myogenin, in human rhabdomyosarcoma sublines. Int J Cancer 1992;50:977–83.
47. Bastien J, Rochette-Egly C. Nuclear retinoid receptors and the transcription of retinoid-target genes. Gene 2004;328:1–16.
48. Drayson MT, Michell RH, Durham J, Brown G. Cell proliferation and CD11b expression are controlled independently during HL60 cell differentiation initiated by 1,25-α-dihydroxyvitamin D_3 or all-*trans*-retinoic acid. Exp Cell Res 2001;266:126–34.
49. Collins SJ. The HL-60 promyelocytic leukemia cell line: proliferation, differentiation, and cellular oncogene expression. Blood 1987;70:1233–44.
50. Minucci S, Nervi C, Lo Coco F, Pelicci PG. Histone deacetylases: a common molecular target for differentiation treatment of acute myeloid leukemias? Oncogene 2001;20:3110–5.
51. Lovat PE, Annicchiarico-Petruzzelli M, Corazzari M, et al. Differential effects of retinoic acid isomers on the expression of nuclear receptor co-regulators in neuroblastoma. FEBS Lett 1999;445:415–9.
52. Reynolds CP, Wang Y, Melton LJ, Einhorn PA, Slamon DJ, Maurer BJ. Retinoic-acid-resistant neuroblastoma cell lines show altered MYC regulation and high sensitivity to fenretinide. Med Pediatr Oncol 2000;35: 597–602.
53. Joshi S, Guleria R, Pan J, DiPette D, Singh US. Retinoic acid receptors and tissue-transglutaminase mediate short-term effect of retinoic acid on migration and invasion of neuroblastoma SH-SY5Y cells. Oncogene 2006;25:240–7.
54. Codina A, Love JD, Li Y, Lazar MA, Neuhaus D, Schwabe JW. Structural insights into the interaction and activation of histone deacetylase 3 by nuclear receptor corepressors. Proc Natl Acad Sci U S A 2005; 102:6009–14.
55. Perissi V, Aggarwal A, Glass CK, Rose DW, Rosenfeld MG. A corepressor/coactivator exchange complex required for transcriptional activation by nuclear receptors and other regulated transcription factors. Cell 2004; 116:511–26.
56. Rosenfeld MG, Lunyak VV, Glass CK. Sensors and signals: a coactivator/corepressor/epigenetic code for integrating signal-dependent programs of transcriptional response. Genes Dev 2006;20:1405–28.
57. Corcoran J, Maden M. Nerve growth factor acts via retinoic acid synthesis to stimulate neurite outgrowth. Nat Neurosci 1999;2:307–8.
58. DiGiovanna JJ. Retinoid chemoprevention in patients at high risk for skin cancer. Med Pediatr Oncol 2001;36: 564–7.

Oncogene (2007) 26, 893–904

www.nature.com/onc

ORIGINAL ARTICLE

Crk-associated substrate lymphocyte type regulates transforming growth factor-β signaling by inhibiting Smad6 and Smad7

S Inamoto[1,2,4], S Iwata[1,4], T Inamoto[1,2,4], S Nomura[1], T Sasaki[1], Y Urasaki[1], O Hosono[1], H Kawasaki[1], H Tanaka[1], NH Dang[3] and C Morimoto[1,3]

[1]Division of Clinical Immunology, Advanced Clinical Research Center, Institute of Medical Science, The University of Tokyo, Tokyo, Japan; [2]Department of Medicine, Osaka Medical College, Osaka, Japan and [3]Department of Hematologic Malignancies, Nevada Cancer Institute, Las Vegas, NV, USA

Crk-associated substrate lymphocyte type (Cas-L) is a 105 kDa docking protein with diverse functional properties, including regulation of cell division, proliferation, migration and adhesion. Cas-L is also involved in β1 integrin- or antigen receptor-mediated signaling in B and T cells. In the present study, we demonstrate that Cas-L potentiates transforming growth factor-β (TGF-β) signaling pathway by interacting with Smad6 and Smad7. Immunoprecipitation experiments reveal that single domain deletion of full-length Cas-L completely abolishes its docking function with Smad6 and Smad7, suggesting that the natural structure of Cas-L is necessary for its association with Smad6 and Smad7. On the other hand, both N-terminal and C-terminal deletion mutants of Smad6 and Smad7 still retain their docking ability to Cas-L, suggesting that Smad6 and Smad7 possess several binding motifs to Cas-L. Moreover, Cas-L interaction with Mad-homology (MH)2 domain, but not with MH1 domain of Smad6 or Smad7, ameliorates TGF-β-induced signaling pathway. Finally, depletion of Cas-L by small-interfering RNA oligo attenuates TGF-β-induced growth inhibition of Huh-7 cells, with a concomitant reduction in phosphorylation of Smad2 and Smad3. These results strongly suggest that Cas-L is a potential regulator of TGF-β signaling pathway.
Oncogene (2007) **26**, 893–904. doi:10.1038/sj.onc.1209848; published online 7 August 2006

Keywords: Cas-L; Smad6; Smad7; TGF-β; cancer

Introduction

β1 integrins exhibit a variety of biological functions through specific interaction with their ligands (Hynes, 1992; Juliano and Haskill, 1993). We previously demonstrated that the 105 kDa protein (pp105) termed Cas-L (Cas lymphocyte type) (Minegishi *et al.*, 1996) or human enhancer of filamentation 1 (HEF1) (Law *et al.*, 1996) is a focal adhesion kinase (FAK)-associated docking protein that is heavily tyrosine phosphorylated by FAK and Src family kinases upon engagement with β1 integrin and the T-cell antigen receptor complex in T cells (Minegishi *et al.*, 1996; Tachibana *et al.*, 1997; Ohashi *et al.*, 1998). Transfection of Cas-L into Jurkat cells markedly enhanced cell motility (Ohashi *et al.*, 1999) and interleukin-2 production (Kamiguchi *et al.*, 1999) following β1 integrin engagement. These results clearly indicate that Cas-L plays a key role in β1 integrin-mediated signal transduction and cell migration.

The transforming growth factor-β (TGF-β) superfamily of cytokines has diverse functional roles during embryonic development and tissue homeostasis (Derynck and Zhang, 2003). Disruption of TGF-β signaling is responsible for a number of developmental disorders (Datta and Moses, 2000), fibrotic diseases (Yagil *et al.*, 2005) and human cancers (Kato *et al.*, 2002). Although TGF-β acts as a tumor suppressor (Kato *et al.*, 2002), it also plays opposite roles in tumor progression. As carcinogenesis proceeds and tumor cells acquire resistance to TGF-β-induced growth arrest, TGF-β accelerates cancer cell progression. Therefore, it is quite important to control the sensitivity to TGF-β for regulation of growth of cancer cells. The TGF-β superfamily transmits signals via cell surface complexes of type I and type II receptor serine/threonine kinase and intracellular Smad transcription factors, which are classified into three functional groups (Derynck and Zhang, 2003). Receptor-regulated Smads and R-Smads (Smad1, 2, 3, 5 and 8) are phosphorylated by type I receptor and oligomerize with the common mediator, Co-Smad (Smad4) (Grönroos *et al.*, 2002; Sugano *et al.*, 2003). These heteromeric complexes are translocated into the nucleus to regulate gene transcription by either association with DNA-binding proteins or direct binding to promoter sequences in target genes (Sugano *et al.*, 2003). On the other hand, inhibitory-Smads, I-Smads (Smads6 and 7) are negative signal regulators that block R-Smad phosphorylation by the type I receptor, concomitantly inducing type I receptor dephosphorylation

Correspondence: Dr C Morimoto, Division of Clinical Immunology, Advanced Clinical Research Center, Institute of Medical Science, University of Tokyo, 4-6-1 Shirokanedai, Minato-ku, Tokyo 108-8639, Japan.
E-mail: morimoto@ims.u-tokyo.ac.jp
[4]These authors contributed equally to this work.
Received 10 March 2006; revised 14 June 2006; accepted 20 June 2006; published online 7 August 2006

and proteasomal degradation (Heldin *et al.*, 1997; Nakao *et al.*, 1997; Chacko *et al.*, 2004).

We recently demonstrated that Cas-L is upregulated in human T-lymphotropic virus type I (HTLV-I) Tax transgenic mice (Miyake-Nishijima *et al.*, 2003), and that Cas-L regulates Tax-nuclear factor-κB pathway by direct interaction with Tax (Iwata *et al.*, 2005). Cas-L was previously reported to be involved in TGF-β signaling pathway. For example, under certain circumstances, TGF-β induces gene transcription and protein expression of Cas-L with no effect on the stability of either Cas-L protein or mRNA (Fashena *et al.*, 2002), whereas in other experimental conditions, TGF-β promotes proteosomal degradation of Cas-L (Zhang *et al.*, 2000). However, the biological significances of Cas-L in TGF-β signaling remain to be clarified. Our search for putative Cas-L associated proteins to further investigate the biological role of Cas-L led to the identification of Smad6 and Smad7, the negative signal regulators of TGF-β signaling pathways. In this study, we determined the functional significance of Cas-L interaction with I-Smads, Smad6 and Smad7. We found that Cas-L facilitates TGF-β signaling, and that the mechanism responsible for this effect appears to be the abrogation of recruitment of I-Smads to TGF-β type I receptor induced by the Cas-L–I-Smads interaction, subsequently, resulting in the acceleration of activated R-Smads by TGF-β. On the basis of our findings, we propose that the Cas-L can confer sensitivity to TGF-β, with implications for cell development, immune response, inflammatory disease and tumor biology.

Results

Cas-L interacts with Smad6 and Smad7

To understand the biological significance of Cas-L, we performed yeast two-hybrid cDNA cloning in search for Cas-L binding proteins as described previously (Iwata *et al.*, 2005). We screened over 1×10^6 independent clones from the cDNA library of the lymphoblastic cell line SLB-I. Among 180 clones selected by histidine auxotrophy and β-galactosidase (β-gal) expression, we identified a clone containing Smad7 cDNA (aa 203–353) in frame with GAL4 activator domain.

We next examined the association of exogenous Cas-L protein with Smad6 and Smad7. Unlike the results from the yeast two-hybrid assay using SLB-I cDNA library, co-transfection study with 293 T cells using flag-tagged Smad6 or Smad7 with c-myc-tagged Cas-L revealed that Cas-L specifically immunoprecipitated with both Smad6 and Smad7 before TGF-β treatment (Figure 1a). This discrepancy arose from the cell-type specific differentially expressed transcripts (Supplementary Figure 1). Moreover, immunoprecipitation study of endogenous proteins revealed that the amount of Cas-L binding to Smad6 was increased with increasing doses of TGF-β (Figure 1b, upper panels). Similarly, endogenous Smad7–Cas-L binding was accelerated by TGF-β treatment (Figure 1b, lower panels).

To further investigate the intracellular events associated with the interaction of these proteins after TGF-β treatment, we next examined colocalization of Cas-L and I-Smads using confocal microscopy. Co-transfection study of flag-tagged Smad7 with c-myc-tagged Cas-L showed that Smad7 and Cas-L were dynamically colocalized in the cytoplasm, but not in the nucleus, following TGF-β treatment, with Smad7 gradually localizing in the cytoplasm (Figure 1c). Colocalization of Smad6 and Cas-L was also upregulated by TGF-β treatment (data not shown). These results thus suggested that Cas-L associates with both Smad6 and Smad7, with the association between Cas-L and both Smad6 and Smad7 being accelerated by TGF-β treatment.

*Cas-L counteracts I-Smads-induced inhibition of transcriptional activity by TGF-*β

As Cas-L interacted with Smad6 and Smad7, we further examined the functional consequences of Cas-L on TGF-β-induced transcriptional activity using reporter assay. As seen in Figure 2a, lane 7, Cas-L merely upregulated the basal (endogenous) transcriptional activity. Importantly, constitutively active activin-receptor-like kinase-5 (ALK5) (a mimicry of TGF-β) exaggerated the Cas-L-induced upregulation of transcriptional activity in a dose-dependent manner, suggesting that Cas-L induced TGF-β-mediated transcriptional activation (Figure 2a, lanes 8 and 9). Smad7 is known to be more potent than Smad6 in inhibiting TGF-β, whereas Smad6 is more potent than Smad7 to another TGF-β superfamily bone morphogenetic protein (Derynck *et al.*, 2001). As seen in Figure 2a, lanes 3–6, Smad7 inhibited transcriptional activity more strongly than Smad6, with constitutively active ALK5 having a markedly enhancing effect. Importantly, Cas-L counteracted the transcriptional inhibition by Smad6 (Figure 2a, lanes 3 and 4 vs lanes 10 and 11) and Smad7 (Figure 2a, lanes 5 and 6 vs lanes 13 and 14). In addition, this effect was strengthened by increasing doses of constitutively active ALK5 (Figure 2a, lane 11

Figure 1 Cas-L interacts with Smad6 and Smad7. (a) C-myc-tagged full-length Cas-L and flag-tagged Smad6 or Smad7 were co-transfected in 293 T cells, followed by immunoprecipitation using anti-flag antibody, subjected to immunoblotting. Upper panel indicates Cas-L precipitates with flag-Smad6 or flag-Smad7, but not with control vector. (b) Huh-7 cells were treated by TGF-β, subsequently subjected to immunoprecipitation by anti-Smad6, or anti-Cas-L, then followed by SDS–PAGE and immunoblotting. Detection of immunoprecipitated proteins were by anti-Smad6 or anti-Cas-L. (c) C-myc-tagged full-length Cas-L and flag-tagged Smad7 were co-transfected in 293 T cells, followed by immunocytochemistry using anti-flag-FITC antibody and anti-c-myc-Cy3 antibody. (a) Dose-dependent effect of TGF-β on Cas-L-I-Smads interaction was assessed by confocal microscope. (b) Merged view of Cas-L (red) and I-Smads (green) with low-dose TGF-β in lower magnification. (c) Merged view of Cas-L (red) and I-Smads (green) with high-dose TGF-β in lower magnification. Scale bar indicates 5 μm.

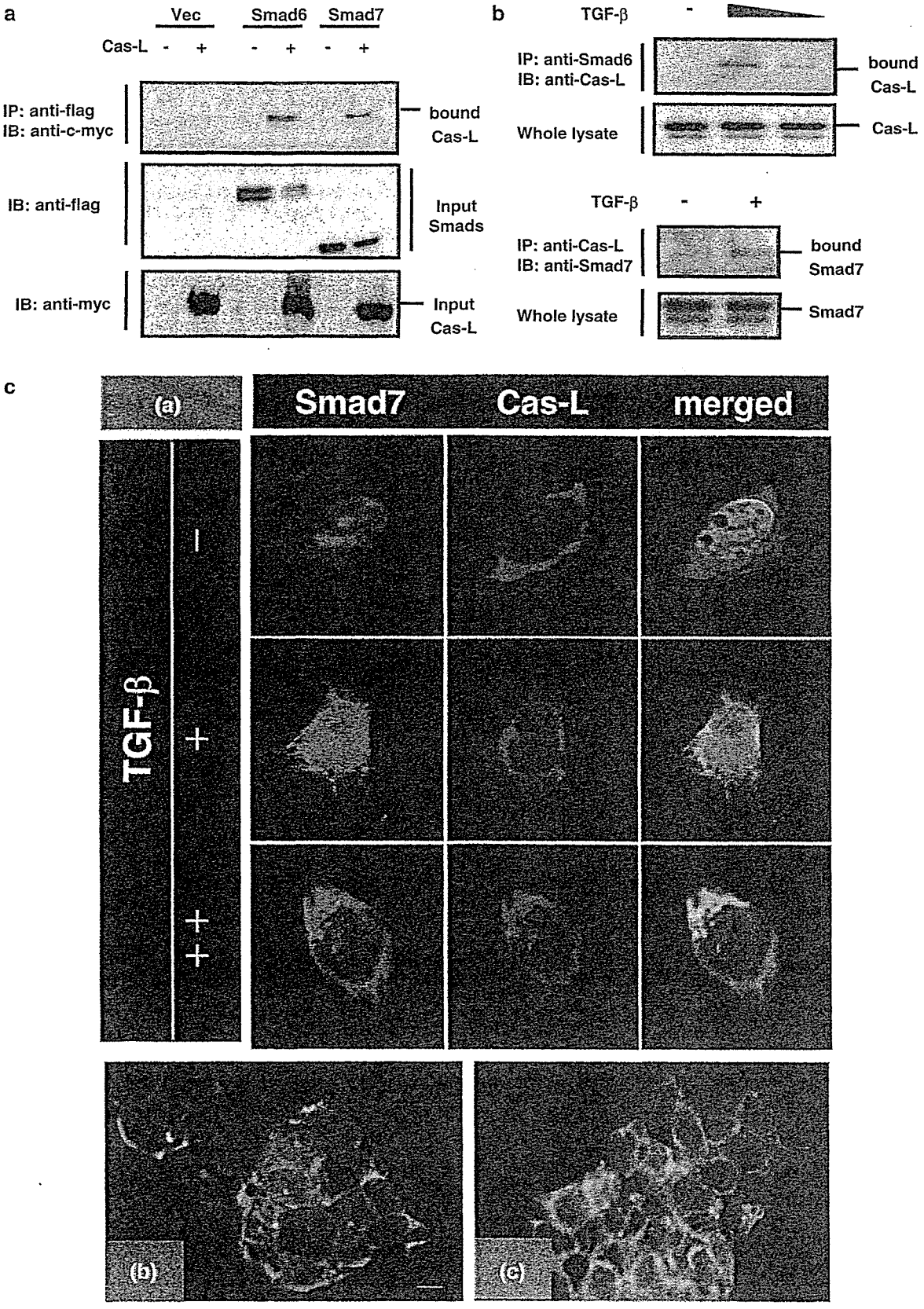
a
Vec
Smad6
Smad7
Cas-L - + - + - +
IP: anti-flag
IB: anti-c-myc
bound
Cas-L
IB: anti-flag
Input
Smads
IB: anti-myc
Input
Cas-L
b
TGF-β -
IP: anti-Smad6
IB: anti-Cas-L
bound
Cas-L
Whole lysate
Cas-L
TGF-β - +
IP: anti-Cas-L
IB: anti-Smad7
bound
Smad7
Whole lysate
Smad7
c
(a)
Smad7
Cas-L
merged
TGF-β
-
+
+
+
(b)
(c)

vs lane 12 and lane 14 vs lane 15). These results suggested that Cas-L counteracts the transcriptional inhibition by I-Smads, and this effect becomes more potent in the presence of ligand stimulation.

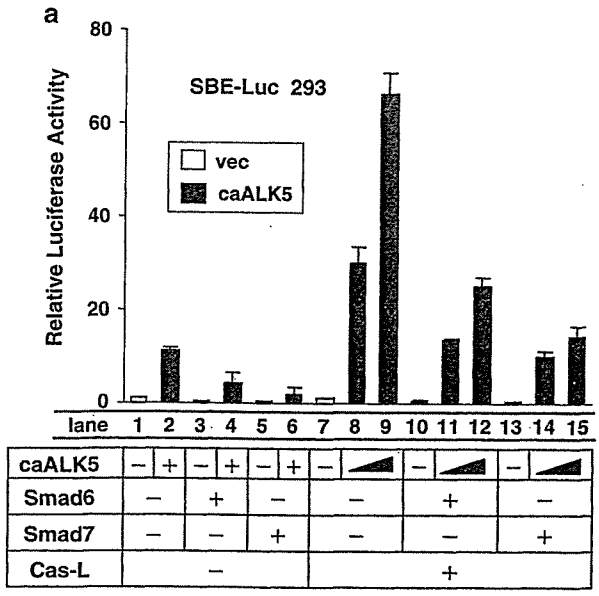

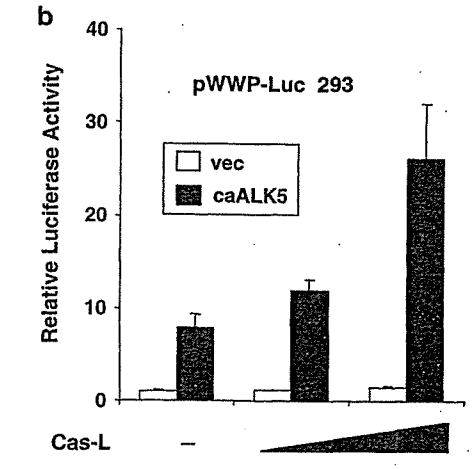

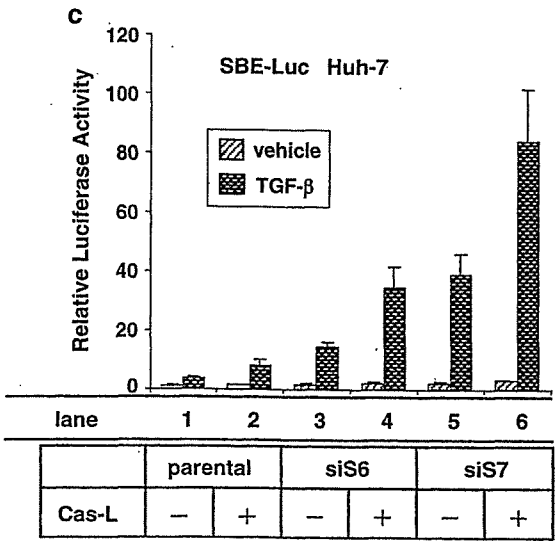

Cyclin-dependent kinase inhibitors, including $p21^{cip1/waf1}$, are known to be the downstream signaling molecules of TGF-β signaling pathway. A reporter plasmid of $p21^{cip1/waf1}$, pWWP-Luc, was employed to evaluate whether Cas-L could perturb the transcriptional activity of $p21^{cip1/waf1}$. As seen in Figure 2b, Cas-L profoundly enhanced pWWP-Luc transcriptional activity in 293 cells compared to the control in a dose-dependent manner, suggesting that abundance of Cas-L is the determinant of transcriptional activation by TGF-β.

Using Huh-7 cells to confirm the results seen in 293 cells, transcriptional activity of SBE-Luc were upregulated with Cas-L co-transfection (Figure 2c, lanes 1 and 2). As expected, small-interfering RNA (siRNA) of both I-Smads induced transcriptional activation by TGF-β (Figure 2c, lanes 3 and 5). It should be noted that the combination of siRNA of Smad6 or Smad7 and Cas-L had an additive or accumulative effect on TGF-β-induced transcriptional upregulation (Figure 2c, lanes 4 and 6). These results suggested that Cas-L upregulates transcriptional activity induced by TGF-β by interfering with I-Smads.

Depletion of endogenous Cas-L by siRNA in Huh-7 cells results in resistance against TGF-β-induced growth inhibition

As overexpression of Cas-L enhanced sensitivity to TGF-β signaling, we examined the effect of Cas-L siRNA oligo-induced depletion of Cas-L on TGF-β signaling. Activation of Smad2 and Smad3 in parental Huh-7 cells occurred from 15 min to 6 h following TGF-β treatment, peaking at 30 min (Figure 3a). Introduction of siCas-L inhibited TGF-β-induced activation of Smad2 and Smad3, with control oligo having no effect (Figure 3b). Expanding on these results, effect of siCas-L on Huh-7 proliferation was assessed. Growth of parental Huh-7 cells was specifically inhibited by TGF-β in a dose-dependent manner (Figure 3c), whereas siCas-L-transfected Huh-7 cells became much less sensitive to TGF-β-induced growth arrest (Figure 3d). These results suggested that Cas-L plays a role in TGF-β signaling pathway, possibly regulating cellular sensitivity to TGF-β.

Figure 2 Cas-L upregulates TGF-β-induced transcriptional activity. Each reporter plasmid was co-transfected with renilla and firefly reporter plasmids as described in Materials and methods. Results with renilla reporter plasmid were used for the normalization of transfection efficiency. (**a**) In 293 cells, SBE-Luc reporter plasmid was transfected with pcDEF6 vector, Smad6 or Smad7 in the presence or absence of constitutive active ALK5. (**b**) In 293 cells, pWWP-Luc reporter plasmid was transfected with pEB6 vector, 0.1 μg Cas-L or 0.2 μg Cas-L in the presence or absence of constitutive active ALK5. (**c**) In Huh-7 cells, or Huh-7 cells with endogenous Smad6 or Smad7 depleted, SBE-Luc reporter plasmid was transfected with pEB6 vector, or Cas-L. At 48 h of transfection, all cells were treated with 1 ng/ml TGF-β. Depletion of endogenous I-Smads was performed as described in Materials and methods.

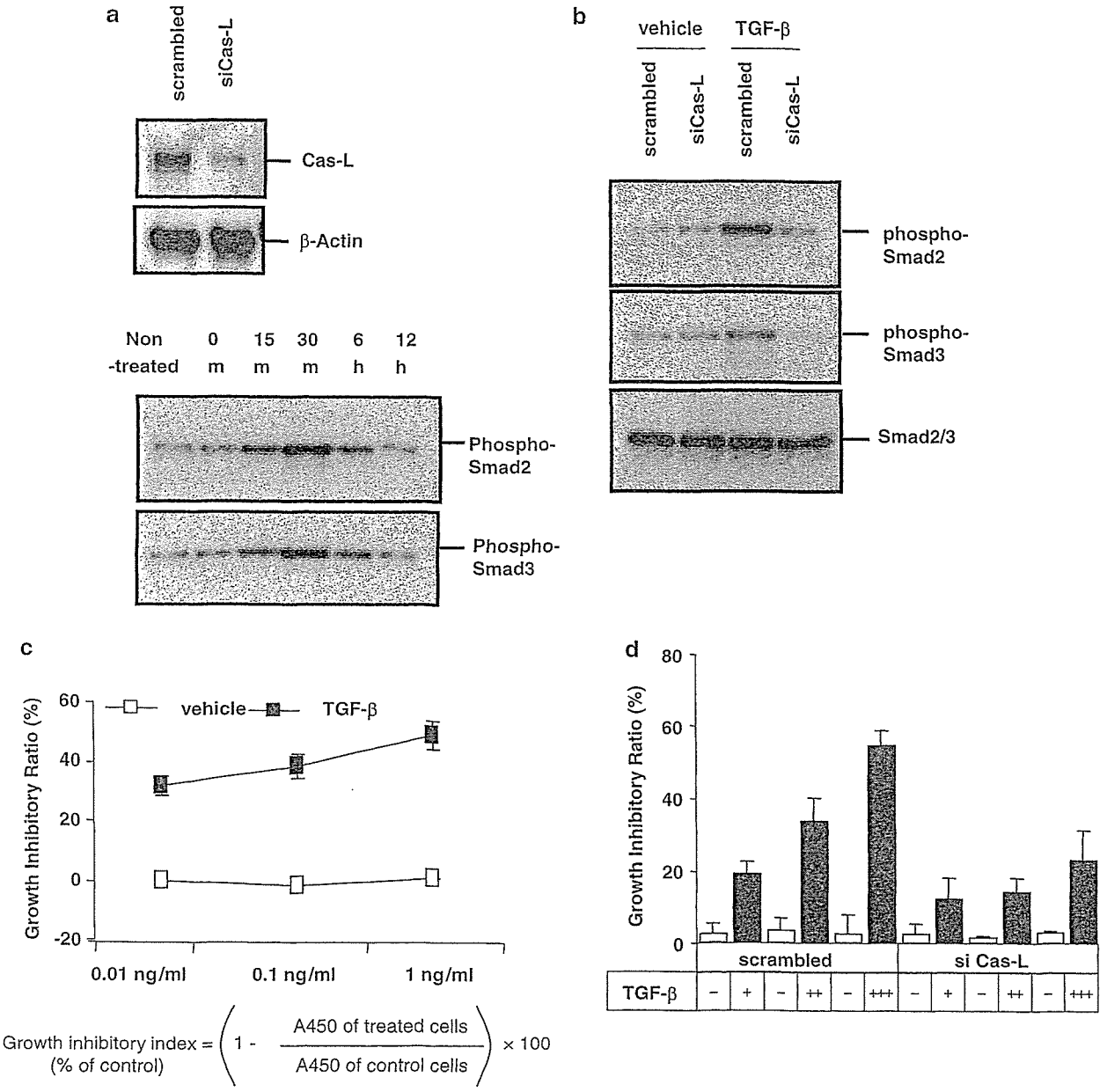

Figure 3 Depletion of Cas-L by siRNA oligo attenuates TGF-β signaling pathway. (a) Upper panel indicates the depletion of endogenous Cas-L in Huh-7 cells. Lower panel indicates time course study of phospho-Smad2 and phospho-Smad3 in TGF-β-treated Huh-7 cells. (b) In Huh-7 cells, phospho-Smad2 and phospho-Smad3 were assessed following TGF-β treatment in the presence of siCas-L or scrambled control. (c) Responsiveness of Huh-7 cells to TGF-β was assessed using *in vitro* proliferation assay. (d) Responsiveness of Huh-7 cells to TGF-β was assessed using *in vitro* proliferation assay with siCas-L or scrambled control.

Full length of Cas-L is necessary for the interaction with Smad6 or Smad7

Cas-L is a multifunctional docking protein with several domain structures specific for Cas family members. To define the particular domain structures of Cas-L necessary for the interaction with Smad6 or Smad7, deletion mutants of each domain or conserved motif of Cas-L protein were constructed. C-myc-tagged full-length Cas-L or mutant Cas-L cDNA subcloned into pEB6 vector was co-transfected with flag-tagged full-length Smad6 or Smad7 in 293 T cells. Full-length Cas-L (Cas-L wild type (wt)) co-precipitated with Smad6 (Figure 4a). Among the various mutants, only Cas-L F co-precipitated with Smad6 and Smad7, although its interaction with these proteins was weaker than Cas-L wt (Figure 4a and b). These results were verified by three independent tests, suggesting that the natural structure of Cas-L itself is necessary for its interaction with Smad6 or Smad7. Expanding on these results, each Cas-L mutant was tested for its effect on sensitivity to TGF-β using an *in vitro* proliferation model. Cas-L wt and Cas-L F enhanced sensitivity of Huh-7 cells to TGF-β, with other mutants and control vector having no effect (Figure 4c). Together with the immunoprecipitation

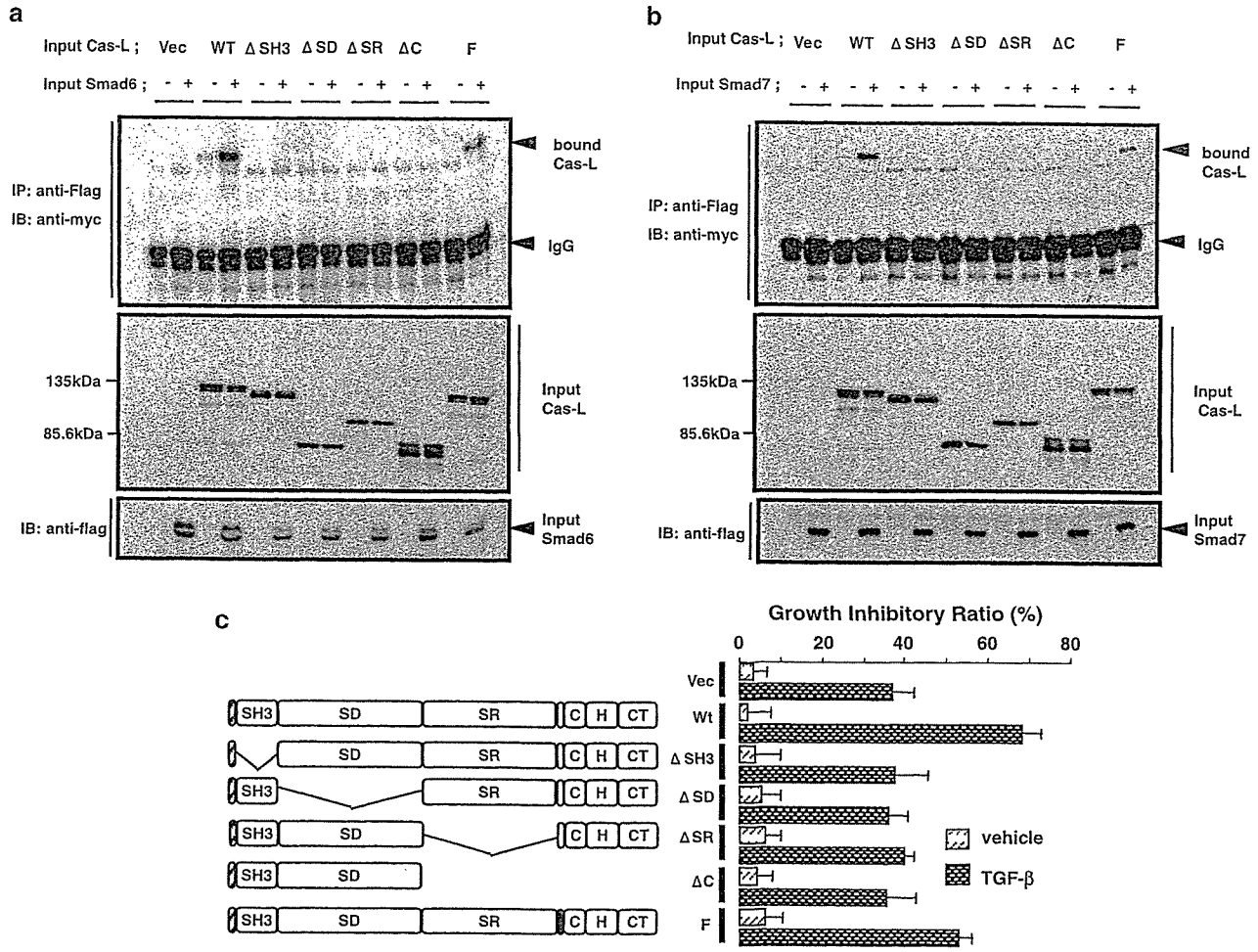

Figure 4 Full length of Cas-L is necessary for physical and functional interaction with Smad6 and Smad7. Each of c-myc tagged full-length Cas-L in a pEB6 vector (Cas-L wt), pEB6-c-myc-Cas-L ΔSH3 domain (Cas-L ΔSH3), pEB6-c-myc-CasL ΔSD domain (Cas-L ΔSD), pEB6-c-myc-CasL ΔSR domain (Cas-L ΔSR), pEB6-c-myc-Cas-L ΔC (Cas-L ΔC) and pEB6-c-myc-Cas-L F, in which Y629 and Y631 were mutated into F (Cas-L F) was co-transfected with pcDEF vector or pcDEF-flag-Smad6/7 in 293 T cells. (a) Lower panel indicates the input Smad6 revealed by immunoblotting using anti-flag antibody. Middle panel indicates the input Cas-L mutants revealed by immunoblotting using anti-c-myc antibody. Upper panel indicates the Cas-L mutants precipitated with Smad6. (b) Lower panel indicates the input Smad7 revealed by immunoblotting using anti-flag antibody. Middle panel indicates the input Cas-L mutants revealed by Western blotting using anti-c-myc antibody. Upper panel indicates the Cas-L mutants precipitated with Smad7. (c) Each Cas-L mutant was assessed for responsiveness of Huh-7 cells to 0.1 ng/ml TGF-β using *in vitro* proliferation assay.

results, these data clearly indicated that Cas-L F was weaker than Cas-L wt in its ability to enhance cellular sensitivity to TGF-β (Figure 4c), hence demonstrating the importance of the natural structure of Cas-L in its interaction with Smad6 or Smad7 and subsequent effect on TGF-β sensitivity.

Both C-terminal and N-terminal of Smad6 and Smad7 can interact with Cas-L

Smad6 and Smad7 have conserved domain structure, namely N-terminal Mad-homology (MH)1 domain and C-terminal MH2 domain (Figure 5a). We next employed flag-tagged Smad6 lacking MH1 domain (Smad6C), flag-tagged Smad6 lacking MH2 domain (Smad6N) and flag-tagged full-length Smad6 (Smad6F) in order to determine the binding domain of Smad6 to Cas-L. Smad7 mutants were also used in the same manner. C-myc-tagged Cas-L was co-precipitated with Smad6F, Smad6C and Smad6N. Likewise, Smad7F, Smad7C and Smad7N were all co-precipitated with Cas-L (Figure 5b).

To further explore the functional significance of the above results, Huh-7 cells co-transfected with mutants of I-Smads and pEB6 vector or Cas-L were subjected to *in vitro* proliferation assay with TGF-β. pEB6 vector plus Smad6F or Smad6C had weaker growth inhibitory effect than pEB6 vector plus pcDEF vector (Figure 5c, lanes 1, 3 and 5). Importantly, Cas-L plus pcDEF vector exhibited additive growth inhibitory effect (Figure 5c, lane 2). Moreover, Cas-L plus Smad6F or Smad6C counteracted the inhibitory effect of Smad6F or Smad6C on TGF-β-induced growth arrest (Figure 5c, lanes 4 and 6). It should be noted that the effect of Cas-L plus Smad6N did not differ from that of pEB6 plus Smad6N (Figure 5c, lanes 7 and 8), indicating that

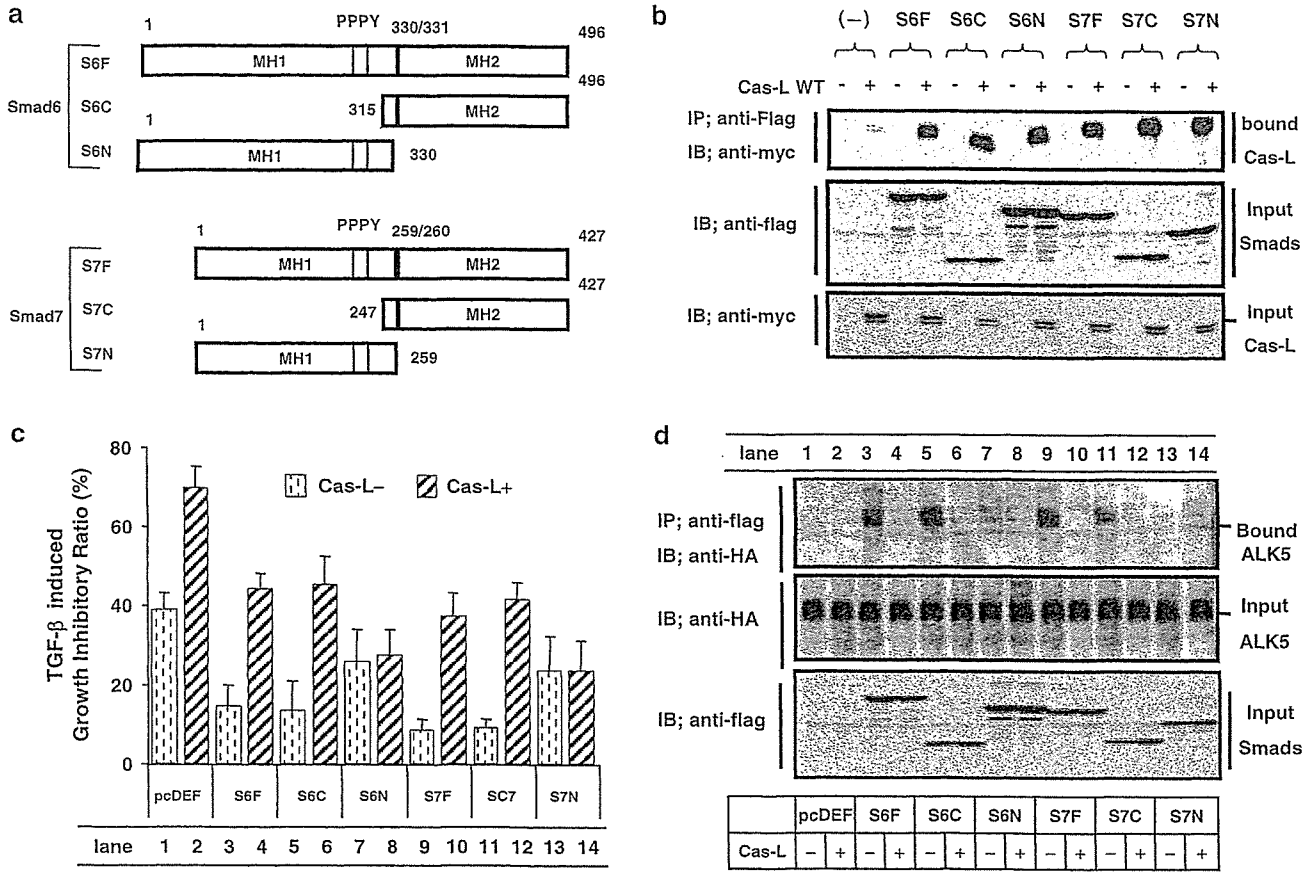

Figure 5 Cas-L interacts physically with MH1 and MH2 domain of Smad6 or Smad7, with MH2 domain playing a key role in TGF-β signaling pathway. (**a**) Flag tagged full-length Smad6 in a pcDEF6 vector (S6F), pcDEF-flag-Smad6 ΔN-terminal MH1 domain lacking aa 1–315 (S6C), pcDEF-flag-Smad6 ΔC-terminal MH2 domain lacking aa 331–496 (S6N), pcDEF-flag full-length Smad7 (S7F), pcDEF-flag-Smad7 ΔN-terminal MH1 domain lacking aa 1–247 (S7C), pcDEF-flag-Smad7 ΔC-terminal MH2 domain lacking aa 1–259 (S7C) was made. (**b**) Lower panel indicates the input full-length c-myc-Cas-L revealed by immunoblotting using anti-c-myc antibody. Middle panel indicates the input flag-Smad6/7 mutants revealed by immunoblotting using anti-flag antibody. Upper panel indicates the Cas-L mutants precipitated with Smad6/7 mutants. Host cell: 293 T cells. (**c**) Each Smad6/7 mutants was assessed in the presence or absence of full-length Cas-L for Huh-7 responsiveness to TGF-β. All mutants were treated with 0.1 ng/ml TGF-β for 24 h, and subsequently tested by *in vitro* proliferation assay. (**d**) Lower panel indicates the input flag-Smad6/7 mutants revealed by immunoblotting using anti-flag antibody. Middle panel indicates the input full-length HA-constitutively active ALK5 revealed by immunoblotting using anti-HA antibody. Upper panel indicates the Smads mutants precipitated with constitutively active ALK5 in the presence or absence of Cas-L. Host cell: 293 T cells.

the interaction between the C-terminal half of Smad6 and Cas-L is important in abrogating the inhibitory role of Smad6 on TGF-β signaling. Similar results were also obtained with the Smad7 model system (Figure 5c, lanes 9–14). These results suggested that Cas-L interacts with both the C-terminal and N-terminal domains of I-Smads, whereas the C-terminal but not the N-terminal of I-Smads has an important role in Cas-L-induced enhanced sensitivity to TGF-β.

Cas-L/C-terminal of I-Smads complex abrogates the recruitment of I-Smads to TGF-β type I receptor

N-terminal and C-terminal of I-Smads differ in their function in TGF-β signaling pathway, with the MH2 domain-containing C-terminal half of Smad6 and Smad7 being responsible for the interaction with TGF-β type I receptor that affects downstream activation of Smad2 and Smad3. Having demonstrated that I-Smads and Cas-L colocalized in the cytoplasm when pulsed by TGF-β (Figure 1c), we hypothesized that Cas-L/I-Smads interaction affects Smad6 or Smad7 binding to TGF-β type I receptor and subsequent inhibition of TGF-β signaling pathway. For this purpose, HA-tagged constitutively active ALK5 (TGF-β type I receptor) and Smad6 or Smad7 mutants were co-transfected into 293 cells. Smad6F, Smad6C, Smad7F and Smad7C were co-immunoprecipitated with constitutively active ALK5 (Figure 5d, lanes 3, 5, 9 and 11), but not Smad6N and Smad7N (Figure 5d, lanes 7, 8, 13 and 14), indicating that the C-terminal half of I-Smad is involved in receptor interaction. However, overexpression of Cas-L inhibited the interaction of I-Smads with constitutively active ALK5 (Figure 5d, lanes 4, 6, 10 and 12), indicating that Cas-L interferes with the association between TGF-β type I receptor and I-Smads.

Taken together, our results strongly suggested that Cas-L is a putative partner of I-Smads, and Cas-L/

I-Smad interaction, mediated by the C-terminal domain of I-Smads, abrogates the recruitment of I-Smads to TGF-β type I receptor, resulting in enhanced sensitivity to TGF-β signaling pathway (Figure 6a–c).

Discussion

In this report, we demonstrated that Cas-L interacts with two different I-Smads, Smad6 and Smad7, to counteract the antagonistic effect of I-Smads on TGF-β signaling. Furthermore, the attenuation of I-Smad function by Cas-L depends on interference with the recruitment of I-Smads to the TGF-β type I receptor.

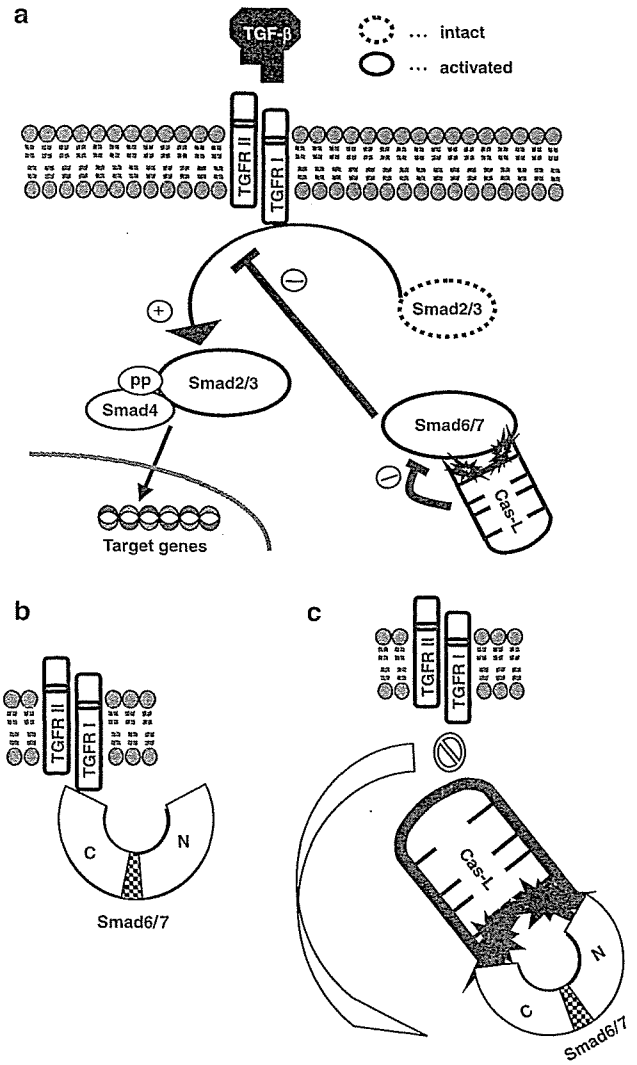

Figure 6 Schematic representation of Cas-L and Smad6/7 interaction. (**a**) TGF-β phosphorylates TGF type II and type I receptor, resulting in the activation of R-Smads, and subsequent homo- or hetero-dimerization with R-Smads or co-Smads. Heterodimerized Smads recruits into the nucleus, subsequently regulating transcriptional activity. I-Smads attenuate the activation of R-Smads. (**b** and **c**) Cas-L interacts with both of MH1 and MH2 domains of Smad6 and Smad7. MH2, but not MH1, domain contains the putative binding sites for the interaction with type I receptor. Cas-L interferes with type I receptor-associated recruiting of Smad6/7 by forming Cas-L–Smad6/7 complex.

Although TGF-β is reported to be a tumor suppressor during carcinogenesis, it also plays an opposite role in some tumors, depending on their origins and stages (Kato *et al*., 2002). This finding suggests the existence of a cellular framework that allows for disruption of subcellular signaling molecules associated with TGF-β involvement in carcinogenesis. For example, certain gastrointestinal tumors have mutations in genes encoding components of the TGF-β signaling pathway, associated with aberrant growth of cancer cells. Defining the molecular basis for TGF-β unresponsiveness in tumors is therefore an important goal in further understanding cancer biology.

Our present work suggests that Cas-L activates TGF-β signaling pathway by interacting with the I-Smads, Smad6 and Smad7. Furthermore, Cas-L upregulates TGF-β-mediated transcriptional activity in gene reporter assays. Notably, genetically introduced Cas-L overcomes the Smad6 and Smad7-induced suppression of TGF-β-mediated SBE-luciferase reporter gene activity in 293 cells, suggesting that the underlying mechanism of Cas-L-induced sensitivity to TGF-β signaling is a loss of I-Smads function. Together with these results, overexpression of Cas-L protein results in an additive sensitivity to TGF-β. In support of this notion, depletion of Cas-L by siRNA oligo overcomes TGF-β-induced growth inhibition in Huh-7 cells, associated with decreased levels of TGF-β-induced phosphorylation of Smad2 and Smad3. Taken together, the above results strongly suggest that Cas-L is a positive regulator of TGF-β signaling.

Importantly, Cas-L interaction with Smad6 and Smad7 depends largely on the full integrity of its protein structure, as mutants lacking SH3 domain, substrate domain, serine-rich lesion and C-terminal all lose their binding affinity for Smad6 and Smad7, whereas only mutant whose Y629 and Y631 residues are mutated into F (FDFVHL) weakly interacts with Smad6 and Smad7. A unique aspect of our data is that the observed Cas-L/I-Smad interaction is not based on specific Cas-L domain, whereas other substrates for Cas-L, including FAK, Crk and Src, interact with its SH3 domain, substrate domain and YDYVHL motif, respectively (Tachibana *et al*., 1997; Ohashi *et al*., 1998). Additional supporting evidence is that only wt Cas-L, and not the mutants lacking the aforementioned domains, affects the sensitivity of Huh-7 cells to TGF-β. Of note is that the addition of the same mutant whose Y629 and Y631 residues are mutated into F (FDFVHL) retains cellular sensitivity to TGF-β.

Although Cas-L mutants except for Cas-L F do not bind to Smad6 and Smad7, all deletion mutants of Smad6 or Smad7 still retain their binding affinity to full-length Cas-L, suggesting that both MH1 and MH2 domains contain the binding motif for Cas-L. The fact that overexpressed Smad6 and Smad7 colocalize with Cas-L predominantly in the cytoplasm suggests that Cas-L/I-Smads interaction induces enhanced sensitivity to TGF-β outside the nucleus. Our work also indicates that Cas-L/I-Smads interaction influences the recruitment of I-Smads to TGF-β type I receptor. In the

absence of Cas-L, overexpressed constitutively active ALK5 (type I receptor) precipitates with full-length Smad6 and Smad7 and MH2 domain of Smad6 and Smad7, but not MH1 domain of Smad6 and Smad7, indicating that the MH2 domain contains the binding motif for ALK5. In the presence of Cas-L, full-length Smad6 and Smad7 and MH2 domain of Smad6 and Smad7 loses their binding affinity to ALK5, with MH1 domain of Smad6 and Smad7 still not binding to ALK5. These data thus indicate that Cas-L interferes with recruitment of Smad6 and Smad7 to TGF-β type I receptor via interaction with the MH2, but not MH1, domain of the I-Smads. Further experiments using affinity crosslinking by labeled TGF-β are being planned to clarify the interaction of I-Smads to TGF-β type I receptor.

A member of the Cas family proteins, which include p130Cas, Efs/Sin and Cas-L/HEF1, Cas-L has a described physiological role at focal adhesion sites (Ohashi *et al.*, 1998). Accumulating evidence strongly suggests that Cas-L is a multifunctional docking protein, with a role in cell motility (van Seventer *et al.*, 2001; Seo *et al.*, 2005), cytokine production (Kamiguchi *et al.*, 1999), cell shape change (Sasaki *et al.*, 2005), cell cycle (Astier *et al.*, 1997) and cell division (Pugacheva and Golemis, 2005), besides cell adhesion. Cas-L overexpression also induces apoptosis in HeLa cells, implying a potential role as a tumor suppressor (Law *et al.*, 2000). As tumor cells can develop resistance to TGF-β-mediated growth inhibition, it is conceivable that Cas-L plays a role in this process. We have found that several cancer cell lines exhibit profoundly impaired endogenous Cas-L (data not shown). In addition, previous work has reported that Huh-7 cells possessing detectable level of Cas-L protein are highly sensitive to TGF-β, whereas Jurkat cells possessing sparse level of Cas-L are not responsive to TGF-β treatment (Hayashi *et al.*, 1997; Lee *et al.*, 2002). It was previously shown that Cas-L binds to R-Smad, Smad3, with being proteasomally degraded by Smad3, and that overexpression of Cas-L in A549 cells results in inhibition of transcriptional activity in TGF-β signaling (Liu *et al.*, 2000). This discrepancy may be explained by that the cell type-specific abundance of subcellular downstream molecules in TGF-β signaling, including R-Smad/I-Smad ratio (Ito *et al.*, 2001), SARA (Xu *et al.*, 2000a) or Ski (Xu *et al.*, 2000b), which differently regulate TGF-β signaling in a complex manner. Moreover, previous work identified a splice variant of Smad6 that is differentially regulated in diseased tissues and appears to be a TGF-β pathway activator, in contrast to wt Smad6 (Krishnan *et al.*, 2001). Further studies are needed to examine the involvement of these molecules with Cas-L/I-Smads interaction in TGF-β signaling. Our data, together with previous work on TGF-β-mediated proteasomal degradation, suggest that the interaction of Cas-L with not only Smad3 but also Smad6 and Smad7, may be an essential part of an endogenous response aimed to limit the consequences of TGF-β refractoriness frequently observed in aggressive cancer cells.

In conclusion, our study indicates that Cas-L is a binding partner for Smad6 and Smad7, and that Cas-L potentiates TGF-β signaling mainly through its interaction with I-Smads. In view of the pivotal roles of TGF-β signaling in the pathophysiology of various diseases, studying Cas-L may therefore shed light on understanding the etiology of such conditions as cancer and connective tissue diseases.

Materials and methods

Reagents and antibodies

Rabbit polyclonal antibody against Cas-L was developed in our laboratory as described previously (Iwata *et al.*, 2005). Anti-c-myc tag monoclonal antibody (mAb) (9E10) was produced from the hybridoma obtained from the American Type Culture Collection (Manassas, VA, USA). Rabbit monoclonal antibodies to phosphorylated forms of Smad2 and Smad3, and mouse monoclonal antibodies to β-actin are all from Cell Signaling Technology Inc. (Beverly, MA, USA). Mouse monoclonal anti-Smad2/3 is from BD PharMingen (Lexington, KY, USA). Anti-Smad6 and Smad7 are from Santa Cruz Biotechnology (Santa Cruz, CA, USA).

Depletion of endogenous Cas-L

To deplete endogenous Cas-L, siRNA-oligo targeting Cas-L cDNA (accession no. NM_006403) was made according to the design site of TAKARA BIO (http://www.takara-bio.co.jp/RNAi.htm); sense: 5′-GGAUGGAUGACUACGAUUA TT-3′, antisense: 3′-TT CCUACCUACUGAUGCUAAU-5′, with its scrambled control oligo which contains the same GC quantity; sense: 5′-UAAUUAGGGUCGGGUAAAC TT-3′, antisense: 3′-TT AUUAAUCCCAGCCCAUUUG-5′. Cas-L siRNA oligo (siCas-L) was transfected using TransIT-TKO transfection reagent (Mirus Bio Corporation, Madison, WI, USA) according to the manufacturer's protocol.

Cells, plasmids and transfection procedures

Huh-7 cells (human hepatocellular carcinoma) were obtained from Cell Resource Center for Biomedical Research, Tohoku University, Sendai, Japan. 293 T cells were obtained from the American Type Culture Collection (Rockville, MD, USA). The plasmid vectors used in exploring signaling pathway were as follows: c-myc tagged full-length Cas-L in a pEB6 vector (Cas-L wt) (pEB6 vector is a kind gift from Y Miwa, University of Tsukuba, Tsukuba, Japan) (Tanaka *et al.*, 1999), pEB6-c-myc-Cas-L ΔSH3 domain lacking aa 1–60 (Cas-L ΔSH3), pEB6-c-myc-CasL ΔSD domain lacking aa 63–401 (Cas-L ΔSD), pEB6-c-myc-Cas-L ΔC lacking aa 406–834 (Cas-L ΔC) and pEB6-c-myc-Cas-L F, in which Y629 and Y631 were mutated into F (Cas-L F), respectively. pcDEF3-Flag (N)-Smad7 (aa 1–427), pcDEF3-Flag-Smad7C (aa 247–427), pcDEF3-Flag-Smad7N (aa 1–259), pcDEF3-Flag-Smad6 (aa 1–496), pcDEF3-Flag-Smad6C (aa 315-496), pcDEF3-Flag-Smad6N (aa 1–330) were provided by Kohei Miyazono as described previously (Hanyu *et al.*, 2001). The plasmids were transfected into cells using FuGENE6 reagent (Roche Diagnostics, Indianapolis, IN, USA).

Yeast two-hybrid screening

The two-hybrid analysis was carried out essentially as described previously (Iwata *et al.*, 2005), using pACTII (for GAL4 activator domain) (Li *et al.*, 1994) and pBTM116 (for LexA DNA-binding domain) (Vojtek *et al.*, 1993). The cDNA

encoding full-length Cas-L was subcloned into pBTM116. The resulting plasmid, pBTM116-Cas-L, was used as bait in a two-hybrid screen of a cDNA library of human HTLV-I infected T cell line (SLB-I) in *Saccharomyces cerevisiae* L40 according to the Matchmaker Two-Hybrid System Protocol (BD Biosciences Clontech, Palo Alto, CA, USA). Positive yeast clones were selected for histidine prototrophy and expression of β-gal. Plasmids containing cDNA clones were rescued from yeast and characterized by DNA sequencing. Concomitantly, those plasmids were introduced back to yeast strain L40 by a polyethylene glycol/lithium acetate method (Bartel *et al.*, 1993). Colonies were grown on selective synthetic medium and were examined for histidine prototrophy and β-gal activity.

In vitro *cell proliferation assay*
Cell proliferation assay was performed as described previously. In brief, cells were incubated in 96-well plates in media alone or in the presence of TGF-β (0.1, 1.0 or 10 ng/ml each) (R&D Systems, Minneapolis, MN, USA), or vehicle control for a total volume of 100 μl (5×10^3 cells/well). After 24 h of incubation at 37°C, Tetra Color ONE solution (Seikagaku, Tokyo, Japan) was added to each well. After another 2 h of incubation, fluorescence intensity was measured at 490 nm using a microplate reader (Bio-Rad, Hercules, CA, USA). All samples were tested in triplicate. Values represent the means of triplicate wells, and the s.e. of the mean was under 15%.

Immunocytochemistry
For fluorescent microscopy experiments using 293T cells, cells were treated and stained according to the methods described previously (Ohnuma *et al.*, 2004). In brief, 293T cells (5×10^4 cells/ml) were grown on coverslips in six-well plates, and transfected with c-myc-tagged Cas-L and Flag-tagged Smad6 or Smad7. The cells were fixed in 4% phosphate-buffered saline-paraformaldehyde solution for 15 min, followed by permeabilization with 0.1% Triton X-100 for 5 min. After blocking with TNB Blocking Buffer (TSA Fluorescence Systems, Perkin-Elmer Life Sciences, Boston, MA, USA), slips were stained with Cy3-labeled anti-c-myc mAb (Sigma, Saint Louis, MO, USA), and fluorescein isothiocynate (FITC)-labeled anti-Flag mAb (SIGMA) over night. After washing, slides were mounted with Prolong Antifade Kit (Molecular Probes, Eugene, OR, USA), and examined by confocal microscope with 40 objective lenses (IX70, Olympus, Tokyo, Japan) using laser excitation at 488 nm.

Immunoprecipitation, SDS–PAGE and immunoblotting
Protein (600 μg) from total cell lysates were diluted in the same final volume of NP-40 buffer (1% NP-40, 0.5% sodium deoxycholate, 5 mM ethylenediaminetetraacetic acid, 50 mM Tris-HCl (pH 8.0), 0.15 M NaCl), containing 1 mM phenylmethylsulfonyl fluoride (PMSF), 10 mM NaF, 1 mM Na_3VO_4, 10 μg/ml aprotinin and 10 μg/ml leupeptin. Corresponding antibodies were added at a final concentration of 2 μg/ml for immunoprecipitation, and immunoprecipitants were subjected to sodium dodecyl sulphate–polyacrylamide gel electrophoresis (SDS–PAGE) and immunoblotting. For detection of phosphorylated proteins, cells were harvested in NP-40 buffer containing 1 mM PMSF, 10 mM NaF, 1 mM Na_3VO_4, 10 μg/ml aprotinin and 10 μg/ml leupeptin. The protein samples were subjected to SDS–PAGE, transferred onto polyvinylidene difluoride membrane (Immobilon-P; Millipore, Bedford, MA, USA). Specific antigens were probed by the corresponding mAbs, followed by horseradish peroxidase conjugated anti-mouse immunoglobulin Ab (Amersham Pharmacia Biotech, Piscataway, NJ, USA). Western blots were visualized by the enhanced chemiluminescence technique (WESTERN LIGHTING, Chemiluminescence Reagent Plus, Perkin-Elmer Life Sciences, Boston, MA, USA).

Luciferase reporter assay
Luciferase reporter assay and transfection procedure were performed as described previously with some modification (Iwata *et al.*, 2005). Briefly, Dual-Luciferase Reporter Assay System (Promega, Madison, WI, USA) was used to measure luciferase activity expressed by the experimental plasmids. Cells were transfected with pWWP-Luc, p3TP-Lux (Cárcamo *et al.*, 1994) and pSBE-Luc using FuGENE6 reagent, according to the manufacturer's instructions. TGF-β was added 24 h after transfection. As internal control, renilla luciferase-expressing plasmid pRL-TK was employed. The enzyme activities of firefly luciferase and renilla luciferase were measured by Luminometer (Model TD-20/20, Turner Design, Inc., Sunnyvale, CA, USA).

Abbreviations

Cas-L, Crk-associated substrate lymphocyte type; TGF-β, transforming growth factor β.

Acknowledgements

This work was supported by Grant-in-Aid of Ministry of Education, Science, Sports and Culture (CM), and Ministry of Health, Labor, and Welfare, Japan (CM). T I is the recipients of a grant from Osaka Kidney Foundation (OKF05-0002), and The Yasuda Medical Foundation. We are thankful to Dr Takeshi Imamura (Department of Biochemistry, The JFCR Cancer Institute, Tokyo, Japan), and Dr Kohei Miyazono (Department of Molecular Pathology, Graduate School of Medicine, University of Tokyo, Japan) for providing us with constructs essential for the present work. We also thank Mr Hiroyuki Kayo for his technical assistance and advices.

References

Astier A, Manié SN, Law SF, Canty T, Haghayghi N, Druker BJ *et al.* (1997). Association of the Cas-like molecule HEF1 with CrkL following integrin and antigen receptor signaling in human B-cells: potential relevance to neoplastic lymphohematopoietic cells. *Leuk Lymphoma* **28**: 65–72.

Bartel P, Chien CT, Sternglanz R, Fields S. (1993). Elimination of false positives that arise in using the two-hybrid system. *Biotechniques* **14**: 920–924.

Cárcamo J, Weis FM, Ventura F, Wieser R, Wrana JL, Attisano L *et al.* (1994). Type I receptors specify growth-inhibitory and transcriptional responses to transforming growth factor beta and activin. *Mol Cell Biol* **14**: 3810–3821.

Chacko BM, Qin BY, Tiwari A, Shi G, Lam S, Hayward LJ *et al.* (2004). Structural basis of heteromeric smad protein assembly in TGF-beta signaling. *Mol Cell* **15**: 813–823.

Datta PK, Moses HL. (2000). STRAP and Smad7 synergize in the inhibition of transforming growth factor beta signaling. *Mol Cell Biol* **20**: 3157–3167.